Applied Ocean Research 154 (2025) 104359

Contents lists available at ScienceDirect

Applied Ocean Research

journal homepage: www.elsevier.com/locate/apor

Influence of the hydraulic power take-off system on the dynamic response and power output of a wind-wave hybrid system

Tiesheng Liu [a,d], Yanjun Liu [a,b,d,e], Shuting Huang [a,c,*], Gang Xue [a,b,d,e]

[a] Institute of Marine Science and Technology, Shandong University, Qingdao 266200, China
[b] School of Mechanical Engineering, Shandong University, Jinan 250061, China
[c] Shenzhen Research Institute of Shandong University, Shenzhen 518057, China
[d] Key Laboratory of High Efficiency and Clean Mechanical Manufacture, Ministry of Education, Jinan 250061, China
[e] National Demonstration Center for Experimental Mechanical Engineering Education, Shandong University, Jinan, 250061, Shandong, China

ARTICLE INFO

Keywords:
WECs micro array
FOWT
Hybrid wind wave system
Hydraulic PTO system
Hydraulic parameters

ABSTRACT

The power take-off (PTO) system plays a crucial role in the wind-wave hybrid system that directly affects the efficiency of wave energy conversion and the relative motion between buoys and the platform. The hydraulic PTO system, a commonly used type of wave energy conversion, has demonstrated practicality and reliability in practical projects. Effects of the hydraulic PTO system on the dynamic response and power output of the hybrid system are unclear due to the limitations of current simulation tools. Therefore, based on potential flow theory, the Laplace equation, blade element momentum theory, and others, this paper proposes an aero-hydro-servo-hydraulic-mooring fully coupled simulation method. The effect of hydraulic parameters (i.e., the piston area, motor displacement, orifice area, equivalent damping, initial volume, and pre-charge pressure) on the hybrid system is studied. The results show that the hydraulic parameters significantly influence the natural periods of heave and pitch of the platform, with variation amplitudes of 14.2 % and 12.27 %, respectively. The phase and amplitude of the PTO force significantly influence the surge, heave, and motion responses of the platform. For deterministic sea states, the same set of hydraulic parameters cannot simultaneously maximize the power generation of the WEC micro array and minimize the pitch motion response of the platform. Hydraulic parameters have negligible effect on the average values of the power generation and rotor torque of the wind turbine, but affect the amplitudes. Furthermore, the established framework can effectively simulate the working process of the hydraulic PTO system in a wind-wave hybrid system, which can provide essential pre-research for the actual hydraulic control to improve the wave energy conversion efficiency and hybrid system stability.

1. Introduction

Under the background of the global consensus on "carbon neutrality", marine renewable energy is developing rapidly (Taveira-Pinto et al., 2020). Among marine renewable energy sources, ocean wind energy and wave energy have abundant reserves and significant potential for development (Turkenburg et al., 2012). Influenced by ecological, channel, fishery, and other factors, offshore wind power is developing from stationary offshore wind turbines to floating offshore wind turbines (FOWTs). However, the excessively high levelized cost of energy (LCoE) for FOWTs and WECs also constrains their commercialization (Astariz and Iglesias, 2015; Blanco, 2009). Based on the close relationship between wind and waves, joint development is regarded as one of the most promising strategies for harnessing marine renewable energy (Cruz, 2007). The combined development of wind and wave energy is often considered to have several potential advantages over the independent development of either wind or wave energy. Through the collaborative development of offshore wind and wave energy, we can enhance the deep utilization of marine renewable resources and improve the efficiency of ocean area usage (Khurshid et al., 2024). At the same time, construction and operational costs are evenly distributed through shared infrastructure and centralized maintenance (Rusu and Onea, 2018). Through the complementary use of wind energy and wave energy, both power generation and the number of effective power

* Corresponding author.
E-mail address: hst@sdu.edu.cn (S. Huang).

https://doi.org/10.1016/j.apor.2024.104359
Received 31 July 2024; Received in revised form 15 October 2024; Accepted 27 November 2024
Available online 4 December 2024

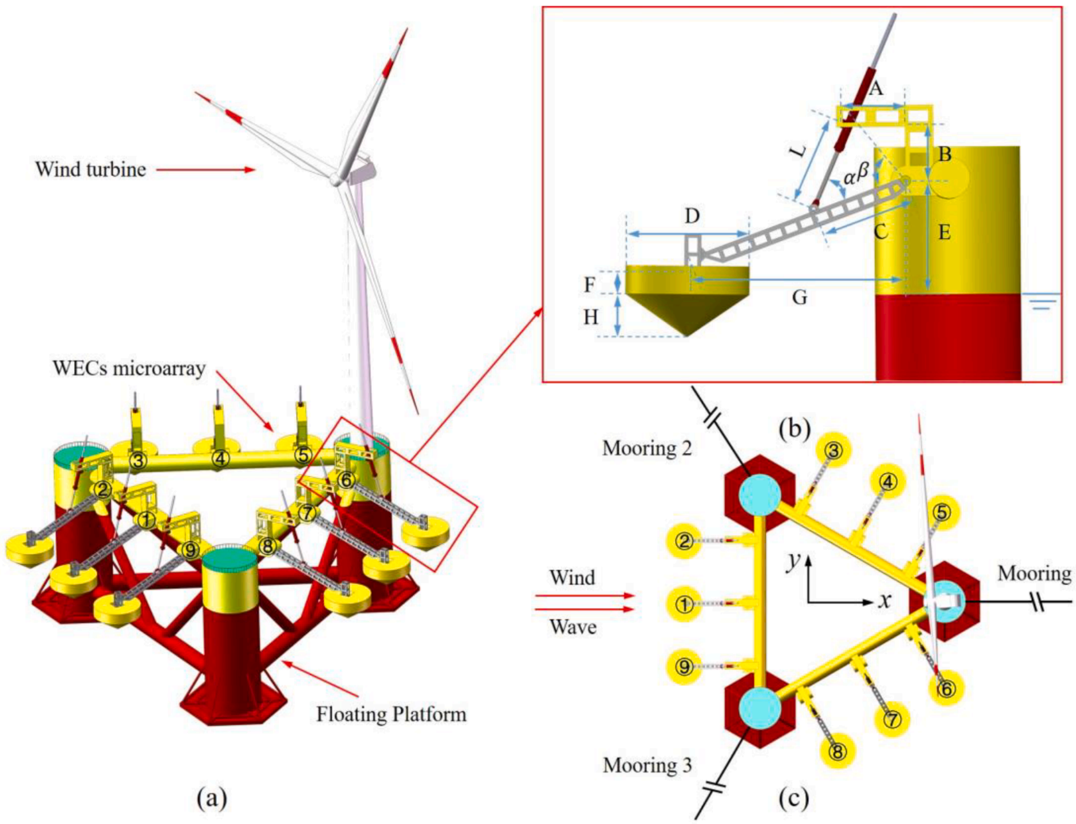

Fig. 1. The wind-wave hybrid system.

generation hours are increased (Perez-Collazo et al., 2019). The WECs can also provide negative damping, which reduces the motion response of the platform and enhances the safety of the system (Zhu et al., 2020).

Therefore, many concepts for wind-wave hybrid systems have been proposed. According to the types of FOWTs, hybrid systems are primarily classified into three categories: the spar wind turbines- wave energy converters (WTs-WECs) system, the semi-submersible WTs-WECs system, and the tension leg platform (TLP) WTs-WECs system (Wan et al., 2024). spar torus combination (STC) (Muliawan et al., 2013) and Wavestar-Hywind (Ghafari et al., 2021) hybrid systems integrate torus and Wavestar technologies with the spar platform, respectively. Submersible WT-WEC hybrid systems, such as the semi-submersible flap combination (SFC) (Michailides et al., 2016), WindWaveFloat (Roddier and Banister, 2012), DeepCwind-Wavestar-combined (DWC) (Si et al., 2021), and W2Power (Legaz et al., 2018), integrate flap-type WECs, oscillating water columns (OWCs), Wavestar WECs, and heave-type WECs onto semi-submersible platforms. TLP WT-WEC hybrid systems, such as the frustum tension leg platform (FTLP-WEC) (Rony and Karmakar, 2024), submerged tension leg platform (STLP-WEC) (Rony and Karmakar, 2023), and traditional TLP-WEC (Konispoliatis et al., 2021), integrate heave-type WECs, OWCs to TLPs, respectively.

In wind-wave hybrid systems, WECs are usually installed on or integrated into a floating platform. The PTO system, as a key component between the energy capture body of WECs and the platform, which directly affects the efficiency of wave energy conversion and the relative motion between buoys and the platform. PTO systems are classified into four primary types: pneumatic, hydraulic, hydrostatic, and direct drive (Falcão, 2007; Bevilacqua and Zanuttigh, 2011; Inoue et al., 1987; Leijon et al., 2006). The hydraulic PTO system is ideally suited for extracting wave energy at low frequencies and high energy densities, which has been proven effective in real sea conditions (Kim et al., 2019). During the development of wind-wave hybrid systems, research has been conducted in various fields. In terms of overall performance evaluation, Jin et al. simplified the PTO system to rotational damping coefficients and subsequently optimized and evaluated the performance of the DeepCWind-Wave-Stars hybrid system (Jin et al., 2023). Chen et al. established a fully coupled model in which the linear damping replaced the PTO system, and evaluated the overall performance of the hybrid system under various wind and wave conditions (Chen et al., 2022). Ghafari et al. simplified the PTO system into a rotary damping coefficient and analyzed the effects of float layout, number, size, and damping coefficient on platform motion response and WEC power capture in the hybrid system (Ghafari et al., 2021; Ghafari et al., 2022). Huang et al. developed a predictive model for the hydraulic PTO system and conducted a multi-objective optimization design for the same system (Huang et al., 2024). Han et al. simplified the PTO system to damping coefficients and evaluated the effects of PTO damping, geometry, and the number of micropores on the performance of the hybrid system (Han et al., 2024). Zhu et al. developed a comprehensive analytical model for a wind-wave hybrid system and compared the overall performance of different types of hybrid systems (Zhu et al., 2024). In terms of PTO control strategies, Si et al. used damping and stiffness coefficients to model PTO systems and studied the effects of three common PTO control strategies on hybrid systems (Si et al., 2021). Borg et al. simulated the control of a PTO system by adjusting damping and stiffness coefficients to achieve the goal of reducing platform motion response and increasing power generation (Borg et al., 2013). Zhang et al. used gain scheduling control schemes to actively control the damping coefficients to reduce the motion of the platform (Zhang et al., 2022). Chen et al. modeled the hydraulic PTO as a Coulomb damping system, which simultaneously enhances power output and reduces motion through effective PTO control (Chen et al., 2024). Yao et al. proposed a hybrid maximum power point tracking (MPPT) control strategy that integrates a wide-range input LLC resonant converter with advanced particle swarm optimization (APSO) to significantly enhance the power generation of WECs (Yao et al., 2023). Stock proposed an

Table 1
Main parameters of the wind-wave hybrid system (Roddier et al., 2010; Liu et al., 2024).

Components	Parameters	Value	Units
Wind turbine	Rotor diameter	126	m
	Hub height	90	m
	Hub diameter	3.0	m
	Rotor mass	1.21×10^5	kg
	Nacelle mass	2.64×10^5	kg
	Tower mass	3.83×10^5	kg
Platform	Column radius	5.35	m
	Column center to center	56.4	m
	Operating draft	22.9	m
	Total platform height	33.6	m
	Length of heave plate edge	13.7	m
	Height of hexagonal damping plate	0.15	m
	Beam diameter	2.0	m
	Diagonal brace diameter	1.8	m
	Total displacement	7.38×10^6	kg
	Platform roll inertia	8.41×10^9	kg·m^2
	Platform pitch inertia	8.41×10^9	kg·m^2
	Platform yaw inertia	9.30×10^9	kg·m^2
Mooring	Number of mooring lines	3	
	Depth to anchors below MSL	42	m
	Mooring line diameter	0.157	m
	Equivalent mooring line mass density	508.5	kg/m
	Equivalent mooring line extensional stiffness	1.9×10^9	N
	Fairlead1	(5.35, 0.0, −7.0)	m
	Fairlead2	(−51.52, 32.83, −7.0)	m
	Fairlead3	(−51.52, −32.83, −7.0)	m
	Anchor1	(467.44, 0.0, −42.0)	m
	Anchor2	(−282.56, 433.01, −42.0)	m
	Anchor3	(−282.56, −433.01, −42.0)	m
WEC	Length of bracket (A)	2.6	m
	Length of bracket (B)	2.36	m
	Length of arm (C)	3.5	m
	Buoy diameter at free surface (D)	8.66	m
	Elevation of hinged structures above Mean Sea Level (MSL) (E)	8.0	m
	Distance from the attachment point of The buoy and swing arm to MSL (F)	1.6	m
	Horizontal distance of hinged Structure to the center of the buoy (G)	8.83	m
	Buoy draft (H)	3.49	m
	Total displacement	7.07×10^4	kg
	Buoy roll inertia	3.31×10^5	kg·m^2
	Buoy pitch inertia	3.31×10^5	kg·m^2
	Buoy yaw inertia	6.13×10^5	kg·m^2

optimal velocity tracking (OVT) control strategy that demonstrated greater power conversion efficiency compared to the adaptive linear damping method (Stock, 2024). In terms of modeling tests, Kamarlouei et al. conducted experiments using rotational friction dampers instead of the PTO system and found that the pitch motion response was reduced by 80 % (Gao et al., 2016). Gao et al. modeled the PTO system with either a pneumatic damper or a hydraulic damper and found that the STC concept would have lower energy costs than the SFC concept (Kamarlouei et al., 2020). In the aforementioned research, while the PTO system model is established using damping and stiffness coefficients or dampers to realize the force and motion transfer between WEC and FOWTs in the hybrid system, the process of hydraulic energy transfer in the PTO system cannot be simulated in detail.

The variation of parameters of different components in the hydraulic PTO system will affect the flow and pressure in the hydraulic pipeline, subsequently influencing the dynamic response and power output of the

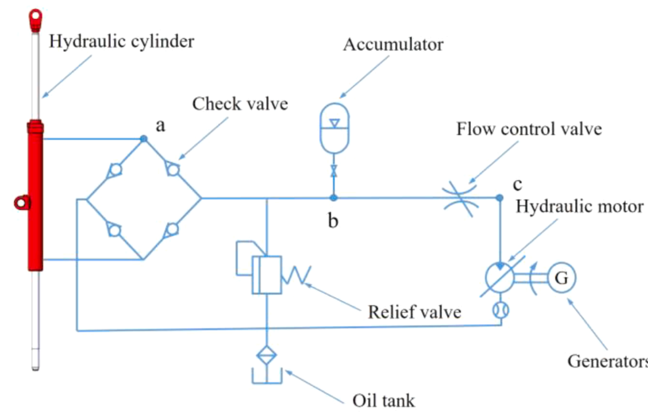

Fig. 2. Principle schematic diagram of the hydraulic PTO system.

hybrid system (Liu et al., 2018; Sricharan and Chandrasekaran, 2021). During the operation of the wind-wave hybrid system, it is necessary to achieve both the improvement of wave energy conversion efficiency and the reduction of platform motion response by controlling the hydraulic components in the hydraulic PTO system. Therefore, it is crucial to clarify the influence of the component parameters of the hydraulic PTO system on the energy acquisition and motion of the hybrid system. Until now, the existing simulation tools have not been able to individually and meticulously analyze the effects of hydraulic PTO systems on platforms, wind turbines, and WECs. Therefore, this study aims to address existing deficiencies by proposing a novel, fully coupled simulation method. The energy transfer and conversion processes of the hydraulic PTO system in a wind-wave hybrid system have been simulated. The influence of hydraulic parameters on the dynamic response and output power of the wind-wave hybrid power system is analyzed. At the same time, the proposed method establishes a foundation for simulating the reduction of motion response and the enhancement of power in the hybrid system during operation. This method can also be applied to comparable hydraulic PTO systems in other wind-wave hybrid systems.

The remainder of this paper is organized as follows. In Section 2, the concept of the wind-wave hybrid system, as well as the main parameters, are described. In Section 3, the basic theory of aero-hydro-servo-hydraulic-mooring full-coupling simulation method is explained and verified. In Section 4, the study analyzes the effects of the main hydraulic component parameters on the natural period and motion response of the platform, power generation of the WECs microarray, as well as the power generation and rotor torque of the wind turbine. In Section 5, the main conclusions are drawn.

2. The wind-wave hybrid system

The wind-wave hybrid system mainly consists of a WindFloat and a WECs micro array, as shown in Fig. 1(a). The WindFloat consists of a 5 MW wind turbine, a semi-submersible platform, and a mooring system. The semi-submersible platform adopts a triangular layout, with three columns as the main floating body positioned at the apex of the triangle. An active ballast system is integrated into the platform to offset the average wind load on the wind turbine. The wind turbine is mounted on the top column of the semi-submersible platform. The mooring system consists of three anchor chains, each with an angle of 120°, as shown in Fig. 1(c). The WindFloat simplifies structural complexity by mounting the wind turbine on a single column. This design has the following advantages, including high turbine versatility, excellent hydrodynamic performance, and a wide range of applications. The WECs micro array comprises a total of 9 WECs evenly distributed around the platform. Each WEC consists of a buoy, a swing arm, a bracket, and a hydraulic PTO system, as shown in Fig. 1(b). The main parameters of the hybrid system are shown in Table 1 (Roddier et al., 2010; Liu et al., 2024). The

Table 2
Main components and parameters ranges.

Main components	Parameters	Default Value	Ranges	Units
Hydraulic cylinder	Piston area	0.035	0.015 ~ 0.05	m^2
Hydraulic motor	Displacement	200	150 ~ 450	mL/rev
Flow control valve	Orifice area	0.0008	0.00005 ~ 0.0012	m^2
Accumulator	Initial volume	120	60 ~ 200	L
	Pre-charge pressure	0.5	0.5 ~ 4.0	MPa
Generator	Equivalent damping	2.866	1.0 ~ 4.5	Nm/(rad/s)

WECs micro array absorb wave energy, thereby reducing the wave loads on the platform. It may also provide negative damping to the platform, thereby reducing its motion response. The integration of the WECs into the FOWT equalizes construction and operational costs, thereby reducing the LoCE. At the same time, it increases the generation capacity and duration, reduces platform motion response, and improves system safety.

Each WEC contains an identical hydraulic PTO system, and the hydraulic schematic is shown in Fig. 2. When the buoy and the platform move relative to each other, the hydraulic cylinder will pump hydraulic oil into the hydraulic pipelines. Through the check valve assembly, the hydraulic oil is rectified. The high-pressure hydraulic oil will flow through the accumulator, the flow control valve, and the hydraulic motor to drive the rotation of the generator. Eventually, the wave energy is converted into electricity. In order to study the influence of the hydraulic PTO system on the dynamic response and power output of the wave hybrid system, this paper focuses on the essential parameters of the main components of the hydraulic PTO system. The main components of the PTO system and their parameter variation range are shown in Table 2.

3. Mathematical model

3.1.1. Multi-body dynamic motion

According to Cummins' theory, the motion equation of the hybrid system in the time domain is (Cummins, 1962),

$$(\boldsymbol{M}+\boldsymbol{A}(\infty))\ddot{\boldsymbol{X}}(t)+\boldsymbol{B}\dot{\boldsymbol{X}}(t)+\boldsymbol{K}\boldsymbol{X}(\boldsymbol{t})+\int_0^t \boldsymbol{h}(t-\tau)\dot{\boldsymbol{X}}(t)\mathrm{d}\tau=\boldsymbol{F}(t) \tag{1}$$

Where $\boldsymbol{M}$ is the mass matrix, $\boldsymbol{A}(\infty)$ is the added mass matrix at infinite frequency, $\boldsymbol{B}$ and $\boldsymbol{K}$ are the damping and stiffness matrix, respectively. $\boldsymbol{X}(t)$ is the displacement matrix. $\boldsymbol{h}(t)$ is the impulse function matrix of the hydrodynamic radiative memory effect, and $\boldsymbol{F}(t)$ is the total external force matrix.

The total external force acting on the floating platform is,

$$\boldsymbol{F}^{\mathrm{FP}}(t)=\boldsymbol{F}^{\mathrm{FP}}_{\mathrm{wave}}(t)+\boldsymbol{F}^{\mathrm{FP}}_{\mathrm{wind}}(t)+\boldsymbol{F}^{\mathrm{FP}}_{\mathrm{moor}}(t)-\boldsymbol{F}^{\mathrm{FP}}_{\mathrm{PTO}}(t)+\boldsymbol{F}^{\mathrm{FP}}_{\mathrm{W}}(t) \tag{2}$$

Where FP and W are marked in the upper right, they represent float platform and WECs micro array, respectively. $\boldsymbol{F}^{\mathrm{FP}}_{\mathrm{wave}}$ is the wave excitation force, $\boldsymbol{F}^{\mathrm{FP}}_{\mathrm{wind}}$ is the aerodynamic load, $\boldsymbol{F}^{\mathrm{FP}}_{\mathrm{moor}}$ is the mooring load, $\boldsymbol{F}^{\mathrm{FP}}_{\mathrm{PTO}}$ is the PTO reaction force.

The total external force acting on the WECs micro array is,

$$\boldsymbol{F}^{\mathrm{W}}(t)=\boldsymbol{F}^{\mathrm{W}}_{\mathrm{wave}}(t)+\boldsymbol{F}^{\mathrm{W}}_{\mathrm{PTO}}(t)+\boldsymbol{F}^{\mathrm{W}}_{\mathrm{FP}}(t) \tag{3}$$

Where $\boldsymbol{F}^{\mathrm{W}}_{\mathrm{wave}}$ is wave excitation force, $\boldsymbol{F}^{\mathrm{W}}_{\mathrm{PTO}}$ is the PTO force, $\boldsymbol{F}^{\mathrm{FP}}_{\mathrm{W}}$ and $\boldsymbol{F}^{\mathrm{W}}_{\mathrm{FP}}$ are the hinged point interaction force, where $\boldsymbol{F}^{\mathrm{FP}}_{\mathrm{W}} = -\boldsymbol{F}^{\mathrm{W}}_{\mathrm{FP}}$.

3.2. Hydrodynamic loads

The hydrodynamic loads acting on floating platforms and WECs micro array are determined by potential flow theory, three-dimensional radiation and diffraction theory, and boundary element method solutions. The fluid is assumed to be inviscid, incompressible and non-rotating. The velocity potential function is obtained by solving Laplace equation (Hess and Smith, 1967),

$$\varnothing\left(\overrightarrow{X},t\right)=a_w\varphi\left(\overrightarrow{X}\right)e^{-i\omega t} \tag{4}$$

Where a_w and ω are the incident wave amplitude and the wave frequency, respectively.

The mutual radiation and shielding effects between floating bodies significantly influence the power generation of WECs and the motion response of the platform. In the hybrid system, the velocity potential function can be expressed as,

$$\varphi\left(\overrightarrow{X}\right)e^{-i\omega t}=\left[\varphi_I+\varphi_d+\sum_{m=1}^{10}\sum_{j=1}^{6}\varphi_{rjm}x_{jm}\right]e^{-i\omega t} \tag{5}$$

Where φ_I and φ_d are the incident potential and the diffraction potential, respectively. φ_{rjm} is the radiation potential due to the unit j-th motion of the m-th structure while other structures remain stationary. the x_{jm} is the amplitude of motion of the j-th degree of freedom of the m-th structure.

The velocity potential function satisfies the following equation,

$$\frac{\partial^2\varphi}{\partial X^2}+\frac{\partial^2\varphi}{\partial Y^2}+\frac{\partial^2\varphi}{\partial Z^2}=0 \tag{6}$$

Linear free surface boundary conditions are defined as follow,

$$-\omega^2\varphi+g\frac{\partial\varphi}{\partial Z}=0 \qquad (Z=0) \tag{7}$$

Body surface boundary conditions are defined as follow,

$$\frac{\partial\varphi}{\partial n}=\begin{cases}-i\omega n_j \ \textit{for radiation potential}\\ -\dfrac{\partial\varphi_I}{\partial n}\ \textit{for diffraction potential}\end{cases} \tag{8}$$

Seafloor surface boundary conditions are defined as follow,

$$\frac{\partial\varphi}{\partial Z}=0 \qquad (Z=-d) \tag{9}$$

After obtaining the potential function, the wave exciting force can be expressed as (Ansys, 2021),

$$\boldsymbol{F}_{jm}=-i\omega\rho\int_{S_{0m}}[\varphi_I+\varphi_d]n_{jm}dS \tag{10}$$

$$\boldsymbol{A}_{jm,kn}+\frac{i}{\omega}\boldsymbol{B}_{jm,kn}=-\frac{i\rho}{\omega}\int_{S_{0m}}\varphi_{rkn}n_{jm}dS \tag{11}$$

where S_{0m} is the m-th mean wetted surface of body. The subscripts m, n correspond to the m-th and n-th structures, and the subscripts j, k refer to the motion modes.

3.3. Aerodynamic loads

FAST uses the blade element momentum theory and a generalized wake model to calculate the aerodynamic loads on the blades. It is assumed that there is no radial interaction between the air streams passing through the field ring.

According to trigonometric functions, the angle of inflow can be expressed as,

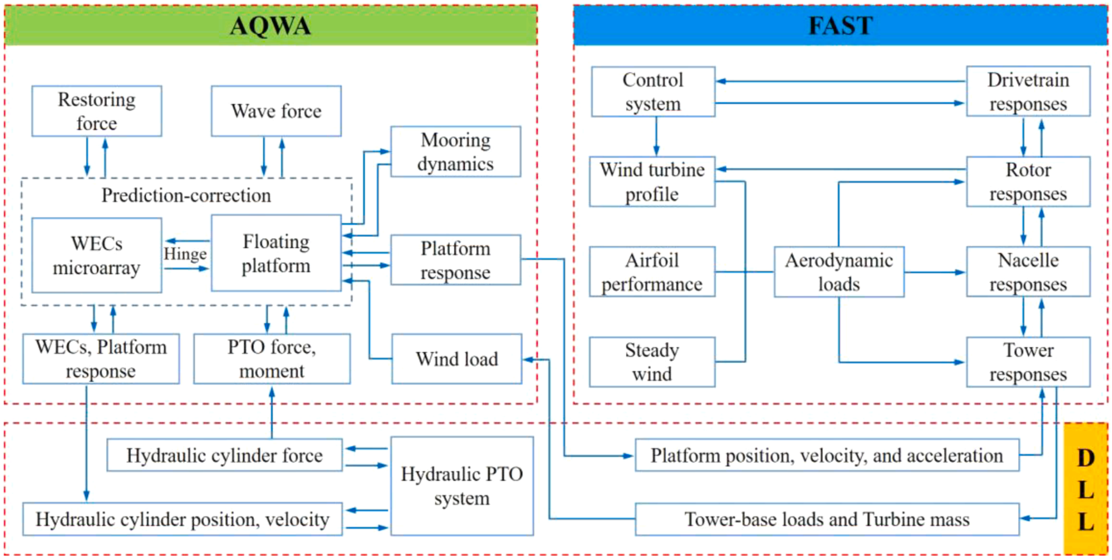

Fig. 3. Aero-hydro-servo-hydraulic-mooring full coupling simulation framework.

$$tan\delta = \frac{V_\infty(1-a')}{\Omega r(1+b')} = \frac{1-a'}{(1+b')\lambda_r} \tag{12}$$

Where δ is the inflow angle, V_∞ is the wind speed flowing from infinity, a' is the axial inducer, b' is the tangential inducer, Ω is the rotor speed, $\boldsymbol{r}$ is the distance between the leaf element and the center of the hub, λ_r is the local tip ratio.

According to the blade element theory, the thrust and torque on the blade element can be expressed as,

$$dT = \frac{1}{2}\rho V_{total}^2(C_l cos\delta + C_d sin\delta\ )c'dr \tag{13}$$

$$dQ = \frac{1}{2}\rho V_{total}^2(C_l sin\delta - C_d cos\delta\ )c'rdr \tag{14}$$

According to the momentum theory, the thrust and torque on the blade element can be expressed as,

$$dT = 4\pi r\rho V_\infty^2(1-a')a'dr \tag{15}$$

$$dQ = 4\pi r^3\rho V_\infty\Omega(1-a')b'dr \tag{16}$$

Where ρ is the air density; V_{total} is the absolute speed; C_l and C_d are the lift and drag coefficients of the airfoil section, respectively; c' is the chord length of the blade element.

The Eqs. (12) and (16) are solved using an iterative method. The axial and tangential induction factors are determined, and subsequently, the aerodynamic load on the blade is calculated. For more information on the theory used to calculate aerodynamic loads on blades in FAST, please refer to the literature (Moriarty, 2005; Jonkman et al., 2015).

3.4. Mooring loads

The centralized mass method is used to calculate the mooring loads of the hybrid system. The mooring cable is divided into a number of segments, with the mass of each segment concentrated at its corresponding node. The equation of motion for each segment of the mooring cable is expressed as follows (Newman, 2018),

$$\begin{cases} \dfrac{\partial \boldsymbol{T}}{\partial S_e} + \dfrac{\partial \boldsymbol{V}}{\partial S_e} + W + \boldsymbol{F}_h = m_e\dfrac{\partial^2 \boldsymbol{R}}{\partial t^2} \\ \dfrac{\partial \boldsymbol{M}}{\partial S_e} + \dfrac{\partial \boldsymbol{R}}{\partial S_e} \times V = -q \end{cases} \tag{17}$$

where $\boldsymbol{T}$ and $\boldsymbol{V}$ are the tension and shear vectors at the first node of the element, respectively; S_e and m_e are the unstretched length of the element and the mass per unit length, respectively; $\boldsymbol{W}$ and $\boldsymbol{F}_h$ are the weight and hydrodynamic load vectors per unit length of the element; $\boldsymbol{R}$ and $\boldsymbol{M}$ are the position and bending moment vectors of the first node of the element; and $\boldsymbol{q}$ is the distributed moment load per unit length of the element.

The bending moment and tension are expressed as follows,

$$\begin{cases} \boldsymbol{M} = EI\cdot\dfrac{\partial \boldsymbol{R}}{\partial S_e} \times \dfrac{\partial^2 \boldsymbol{R}}{\partial S_e^2} \\ \boldsymbol{T} = EA\cdot\varepsilon \end{cases} \tag{18}$$

where EI and EA are the bending stiffness and axial stiffness of the mooring line, respectively; ε is the axial strain of the element.

To ensure that Eq. (16) has a unique solution, fixed boundary conditions are imposed at both the top and bottom ends, which can be expressed as follows,

$$\begin{cases} \vec{\boldsymbol{R}}(0) = \vec{\boldsymbol{P}}_{bot} \\ \vec{\boldsymbol{R}}(L) = \vec{\boldsymbol{P}}_{top} \\ \dfrac{\partial^2 \vec{\boldsymbol{R}}(0)}{\partial S_e^2} = \vec{0} \\ \dfrac{\partial^2 \vec{\boldsymbol{R}}(L)}{\partial S_e^2} = \vec{0} \end{cases} \tag{19}$$

where are the $\vec{\boldsymbol{P}}_{bot}$ and $\vec{\boldsymbol{P}}_{top}$ are the locations of the cable attachment points, L is the total unstretched length of the cable. More details on the theory used to calculate mooring loads in AQWA can be found in references (Ansys, 2021).

3.5. Hydraulic PTO system

The hydraulic cylinder is hinged to the swing arm and platform bracket, and the force of the hydraulic cylinder on the swing arm and platform is,

$$F_{PTO} = P_a A_p \tag{20}$$

Where P_a the pressure at point a, A_p is the piston area of the hydraulic cylinder. Neglecting the opening pressure of the check valve, the pressure at points a and b is considered to be the same.

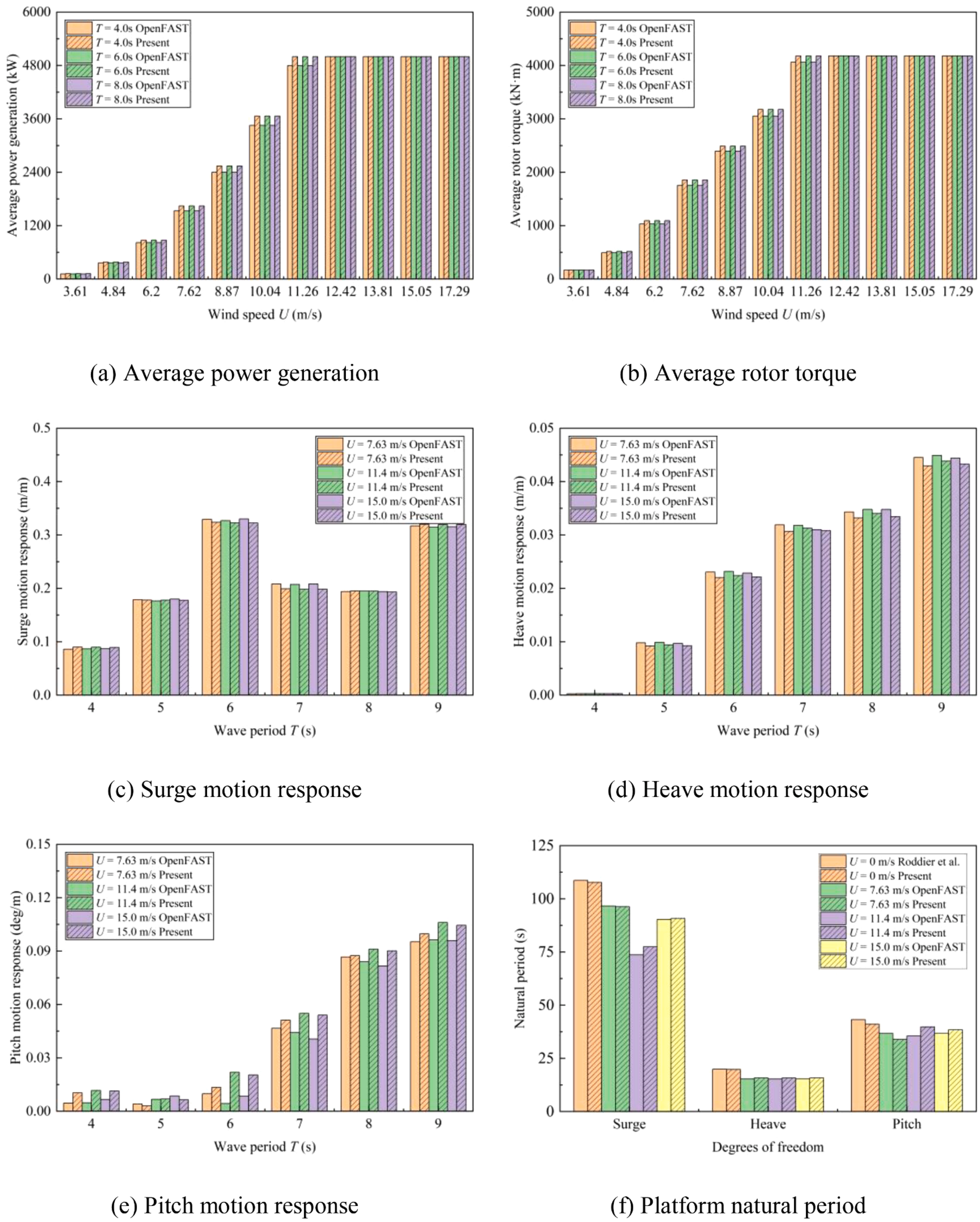

Fig. 4. Comparison of simulation results between OpenFAST and FAST to AQWA.

The equivalent moment acting on the swing arm is,

$$\tau_{PTO} = lF_{PTO}\sin(\alpha) \tag{21}$$

where τ_{PTO} is the equivalent moment, F_{PTO} is the PTO force on the swing arm, l is the length of the force arm, and α is the angle between the hydraulic cylinder and the swing arm.

The speed of movement of the hydraulic rod is,

$$V_h = l\theta\sin(\alpha) \tag{22}$$

Where θ is the angular velocity of the swing arm rotating relative to the platform.

When hydraulic oil flows through hydraulic pipelines and components, the loss of flow and pressure caused by leakage and other factors is ignored. During the reciprocating motion of the hydraulic rod, the flow rate into the hydraulic PTO pipelines is,

$$Q_a = |V_h|A_p \tag{23}$$

The flow rate through the accumulator is,

$$Q_b = Q_a - Q_c \tag{24}$$

Where Q_c is the flow rate through the flow control valve.

The flow rate through the motor is,

$$Q_c = D_m N_m \tag{25}$$

Where D_m is the motor displacement, and N_m is the motor speed.

The relationship between pressure and flow rate at both ends of the

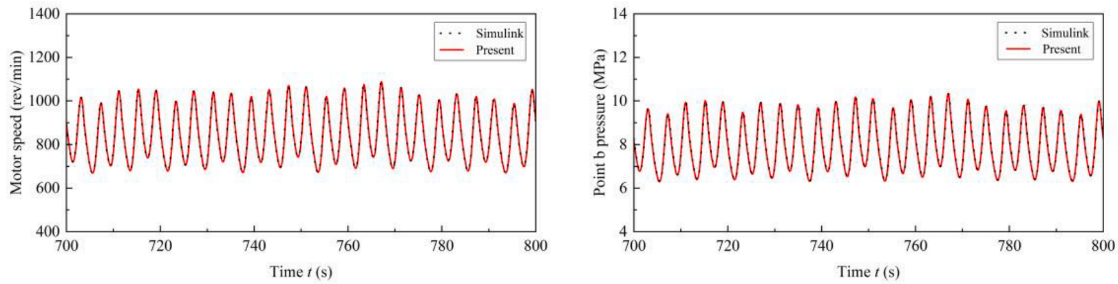

(a) Motor speed (b) Pressure at point b

Fig. 5. Simulation results of pressure at point b and motor speed.

Table 3
Simulation conditions.

Simulation conditions	Environmental parameters			
Free decaying motion	Deviation from the initial position			Wind speed
	Surge 3m	Heave 3m	Pitch 5°	7.63m/s, 11.4m/s, 15m/s
Regular wave	Wave			Wind speed
	Period 4s~9s	Wave height 1m		7.63m/s

flow control valve is (So et al., 2015),

$$Q_c = C_d A_f \sqrt{\frac{2\Delta p}{\rho_h}} \tag{26}$$

Where C_d is the flow coefficient ($C_d = 0.61$), A_f is the orifice area, Δp is the pressure difference between points b and c in the pipeline, and ρ_h is the density of the hydraulic oil.

The pressure at point b in the pipeline is (So et al., 2015),

$$P_b = \frac{P_0}{\left(1 - \frac{V_t}{V_0}\right)^{\kappa}} \tag{27}$$

Where P_0 is the pre-charge pressure, V_0 is the initial volume, V_t is the volume of hydraulic oil in the accumulator, and κ is the multivariate index ($\kappa = 1.4$).

The torque of the hydraulic motor is,

$$T_m = \frac{P_c D_m}{2\pi} \tag{28}$$

Where P_c is the pressure at the point c.

The torque of the generator is,

$$T_g = N_g C_g \tag{29}$$

Where N_g is the motor speed, which is equal to the motor speed, and C_g is the generator damping.

The moment balance equation for the hydraulic motor shaft system is,

$$T_m = J_m \dot{N}_m + T_g \tag{30}$$

Where J_m is the equivalent rotational inertia on the motor shaft, $\dot{N}_m$ is the acceleration of the motor speed, T_g is the generator torque.

The Runge-Kutta method is used to solve Eqs. (23)–(29) simultaneously. The values of P_b and N_m are obtained at each time in the system of equations.

The output power of the hydraulic motor is,

$$P_m = \frac{2\pi T_m N_m}{60} \tag{31}$$

3.3. Full coupling simulation framework

By integrating the hydraulic PTO system model into the FAST-to-AQWA framework (Yang et al., 2020), an aero-hydro-servo-hydraulic-mooring fully coupled simulation method is established. The combination and data interaction process of AQWA and FAST in the fully coupled simulation method are shown in Fig. 3. Based on the information of wind speed and platform displacement, velocity, and acceleration, FAST calculates the aerodynamic force. According to Eqs. (20)–(30), the hydraulic PTO model is built in the dynamic link library (DLL). The hydraulic PTO model calculates the pressure and motor speed of each hydraulic PTO system in the WECs micro array based on the displacement and velocity information of the buoy and platform. Then, the PTO force between the swing arm and the platform is calculated and transferred to each based on the hydraulic PTO system pressure. The information about movement and force between the platform, wind turbine, and hydraulic PTO system is transmitted through DLL.

3.4. Verification

3.4.1. Aero-hydro-servo-mooring coupling

Taking WindFLOAT as an example, the coupling results of OpenFAST and this method are compared to verify the successful integration of FAST into AQWA. The main parameters of WindFLOAT are presented in Table 1 and reference (Roddier, 2011). The wind and waves are incident in the same direction, which is along the x-axis. The wave height $H = 1$ m. The wave period $T = 4$~9 s, with an interval of 1 s. The wind speed is $U = 3.61$~17.29 m/s. It should be noted that the ballast system of the platform is adjusted before the simulation to balance the wind loads generated by varying wind speeds. The comparison of the results for the average wind turbine power generation, average rotor torque, platform motion response, and natural period is shown in Fig. 4. Overall, the results of the coupling framework and OpenFAST are in good agreement, that indicates that FAST has been successfully integrated into AQWA.

3.4.2. Hydraulic PTO system

According to the hydraulic principle schematic diagram (Fig. 2), the hydraulic PTO system is modeled in Simulink. In the fully coupled simulation, the wave and the wind are incident in the same direction, which is along the x-axis. The wave height $H = 1$ m, wave period $T = 8$ s, and wind speed $U = 7.63$ m/s. Taking PTO1 in the hybrid system as an example, the speed of the hydraulic cylinder movement in the PTO1 system is applied to the hydraulic PTO model in Simulink. The fully coupled framework simulation results and Simulink simulation results are shown in Fig. 5. The pressure at point b and the motor speed are in good agreement, indicating that an accurate hydraulic PTO system model has been established in the fully coupled framework.

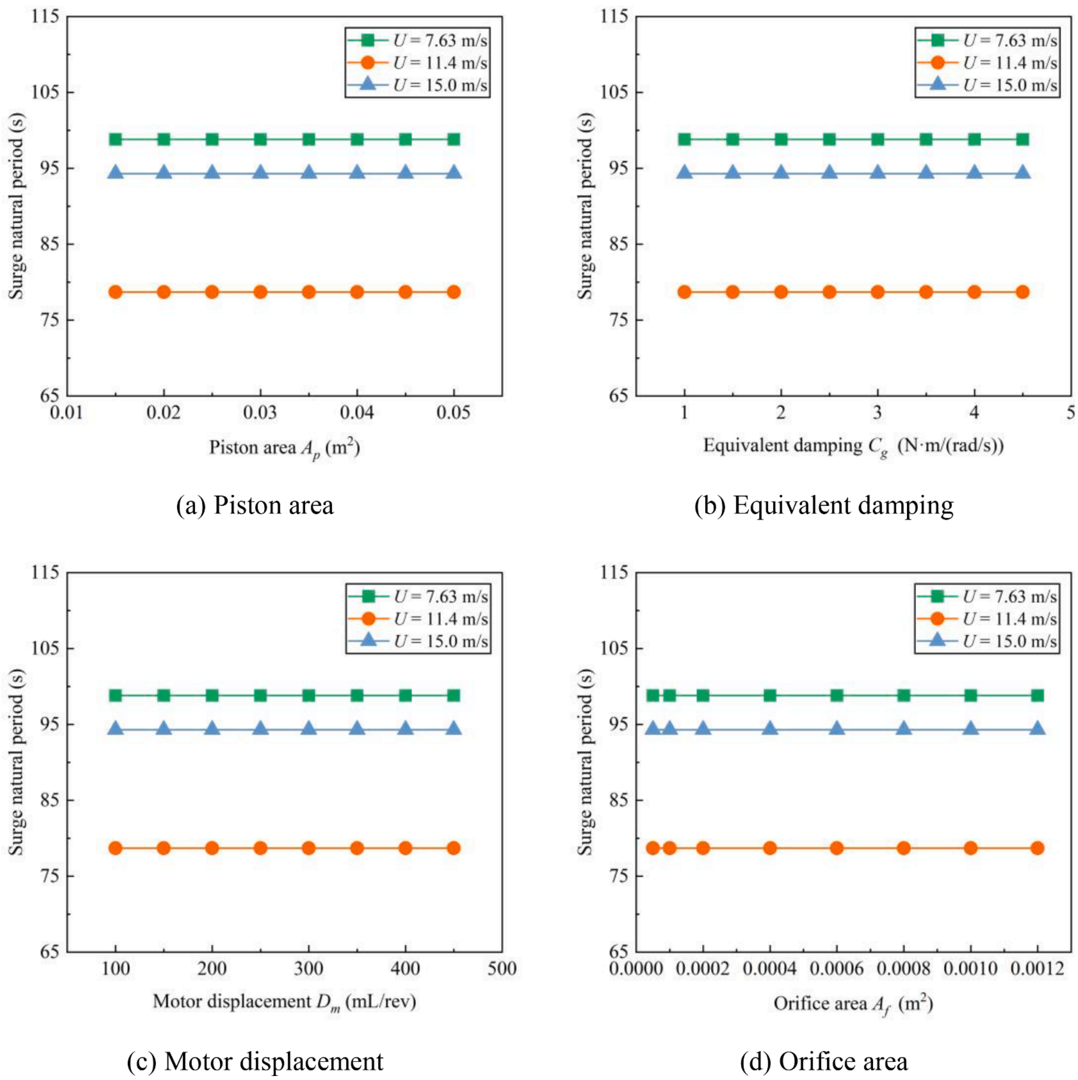

Fig. 6. The influence of hydraulic parameters on the surge natural period.

4. Numerical results and discussions

The variation of component parameters in a hydraulic PTO system will affect the flow and pressure in the pipeline. The fluctuation of pressure will affect the forces exerted between the buoy and the platform, thereby affecting the dynamic response and power output of the hybrid system. This paper analyzes the effect of hydraulic component parameters (i.e., the piston area, motor displacement, orifice area, equivalent damping, initial volume and pre-charge pressure) on the natural period and motion response of a platform, the power generation of WECs micro array, as well as the power generation and rotor torque of the wind turbine. During the simulation process, both the regular wave and the uniform wind incident in the same direction. The component parameters of each hydraulic PTO system in the WECs micro array are identical. The default parameters and the range of variation are shown in Table 2. The wind-wave hybrid system will be deployed in the northern sea area of Weihai, Shandong Province, China (122° E, 38° N). Based on the wind and wave statistics of the deployment sea area (Liu et al., 2024), the simulation working conditions are determined, as shown in Table 3.

4.1. Effect on the platform natural period and motion response

4.1.1. Effect on the platform natural period

The integration of the WECs micro array onto the WindFLOAT will result in a change to the natural period of the platform (Si et al., 2021). The hydraulic PTO system affects the relative motion of the buoy and platform in the hybrid system. Therefore, free decay simulations are conducted with various hydraulic parameters to explore the effects of piston area, motor displacement, orifice area, and equivalent damping on the natural period of the platform. By numerically simulating the free decay test of a hybrid system, the time interval between adjacent wave crests represents the natural period of that degree of freedom.

In Fig. 6, the piston area, motor displacement, orifice area, and equivalent damping have negligible effect on the surge natural period. The effect of pressure variation in the hydraulic pipeline on the surge natural period is negligible. This is mainly because the variation of hydraulic component parameters in the PTO system has negligible influence on the additional mass and stiffness of the hybrid system in terms of surge degrees of freedom. The surge natural period is different at different wind speeds. Since the stiffness of the surge natural period is mainly provided by the mooring system. The hybrid system moorings are subject to varying levels of tension due to wind loads at different wind speeds. Among the three wind speeds, the thrust exerted on the wind turbine is greatest at the rated wind speed (Roddier et al., 2010).

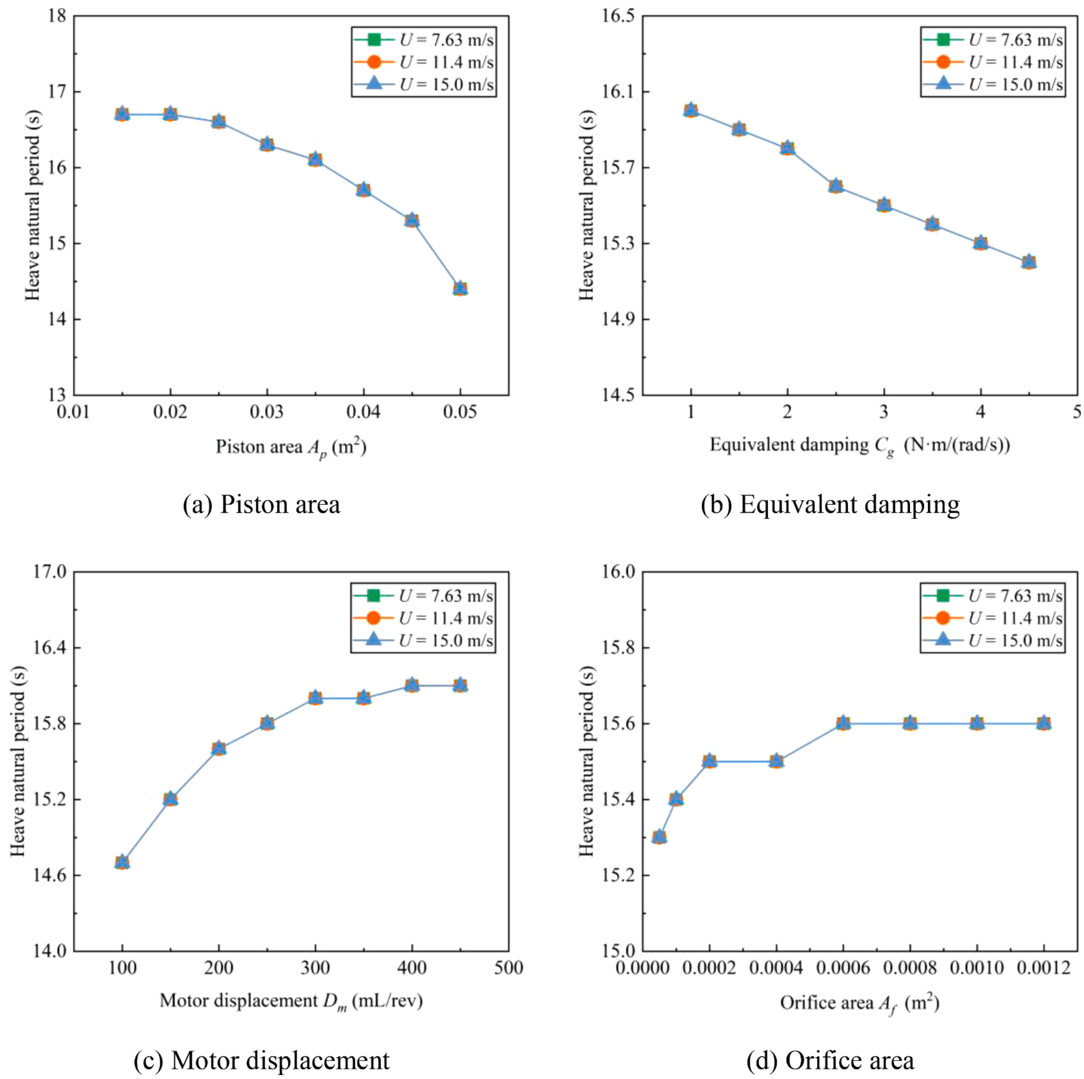

Fig. 7. The influence of hydraulic parameters on the heave natural period.

The stiffness provided by the mooring system is also the largest and therefore the surge natural period is the smallest.

In Fig. 7(a), (b) and 8(a), (b), the heave and pitch natural period decreases with increasing piston area and equivalent damping. In Fig. 7 (a) and 8 (a), when the wind speed $U = 7.63$ m/s, the heave and pitch natural periods decrease by 14.2 % and 7.2 %, respectively. In Fig. 7(b) and 8 (b), when the wind speed $U = 7.63$ m/s, the heave and pitch natural periods decrease by 5 % and 4.1 %, respectively. As the piston area or equivalent damping increases, the pressure at point b in the hydraulic PTO system changes. The PTO forces acting on the platform and buoy gradually increase, and the hydraulic PTO system restricts the relative motion of the platform and buoy. The WECs micro array provide greater equivalent stiffness for heave and pitch motions of the hybrid system platform.

In Fig. 7(c) and 8 (c), the heave and pitch natural periods increase as the motor displacement gradually increases. When the wind speed $U =$ 7.63 m/s, the heave and pitch natural periods increase by 9.52 % and 12.27 %, respectively. In Fig. 7(d) and 8 (d), when the orifice area is small, the variation of the orifice area affects the heave and pitch natural period. As the orifice area increases, the heave and pitch natural period are almost unaffected. When the wind speed $U = 7.63$ m/s, the heave and pitch natural periods increase by 1.96 % and 2.61 %, respectively. As the motor displacement or orifice area increases, the pressure at point b in the hydraulic PTO system gradually decreases. The PTO force acting on the platform and the buoy gradually decreases, and the suppression effect of the hydraulic PTO system on the relative motion of the platform and the buoys gradually decreases. The equivalent stiffness provided by the WECs micro array for the heave and pitch motions of the hybrid system platform also gradually decreases Fig. 8.

4.1.2. *Effect on the platform motion response*

The hydraulic PTO system applies a reaction force to the platform during the conversion of wave energy into electrical energy, which effects the motion response of the platform. Numerical simulations are conducted with various hydraulic parameters to study the effects of piston area, motor displacement, orifice area, equivalent damping, initial volume, and pre-charge pressure on the surge, heave, and pitch motions of the hybrid system platform.

In Figs. 9(a), (b), (c), 10(a), (b), (c), and 11(a), (b), (c), when the period is the same, the piston area and equivalent damping have the same effect on the surge, heave, and pitch motions of the platform. The pressure at point b in the hydraulic PTO system varies as the piston area and equivalent damping increase. The reaction force on the platform from the hydraulic PTO system gradually increases. Comparing with the piston area and equivalent damping, the motor displacement has the opposite effect on the surge, heave, and pitch motions of the platform. The pressure at point b in the hydraulic PTO system decreases as the motor displacement increases, consequently reducing the reaction force

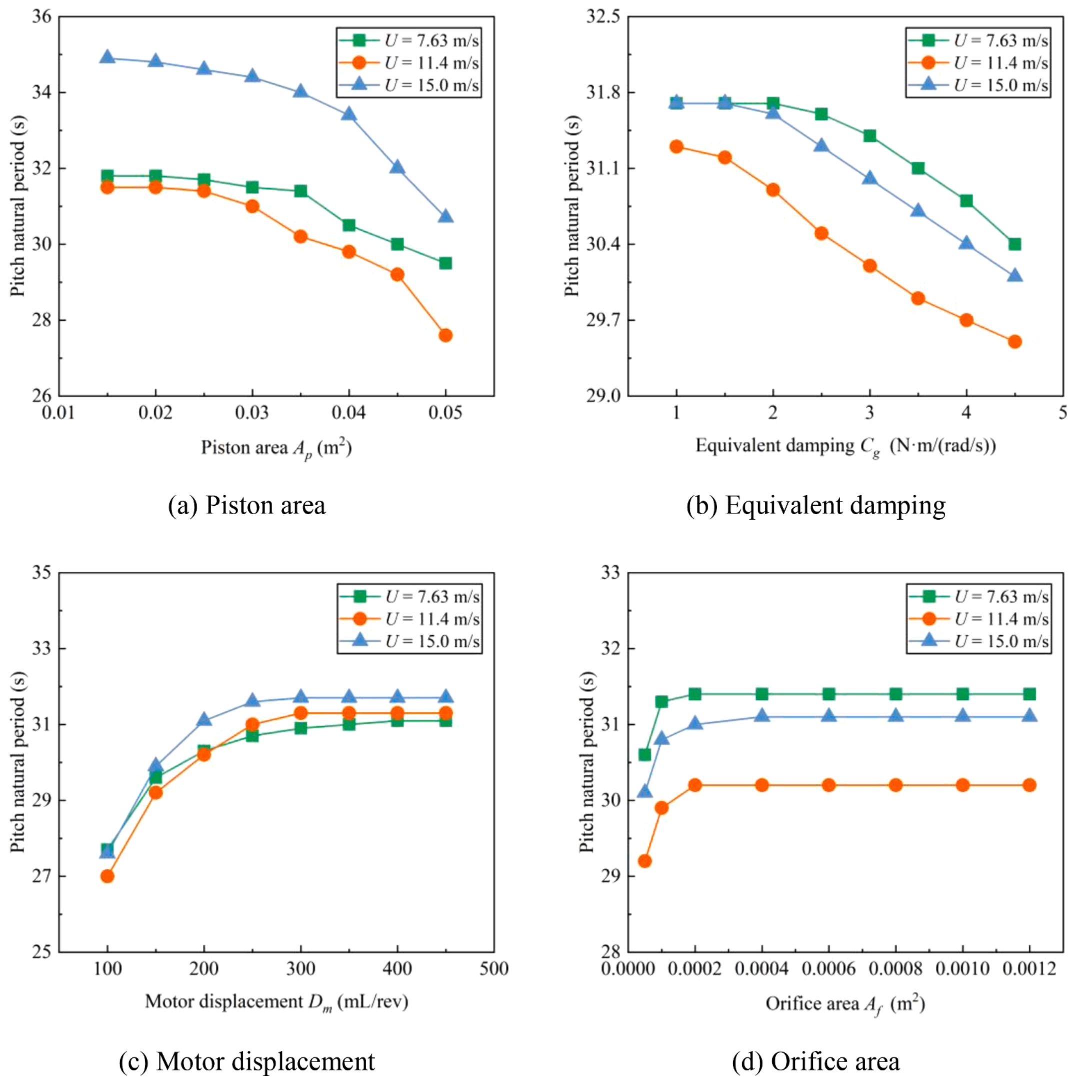

Fig. 8. The influence of hydraulic parameters on the pitch natural period.

on the platform. When the sum of PTO reaction force and the wave excitation force are close to each other in phase, the increase of the total reaction force will worsen the surge, heave, and pitch motions of the platform. Conversely, when they are out of phase, the surge, heave, and pitch motions of the platform will decrease.

In Figs. 9(d), 10(d), and 11(d), when the orifice area is small, it has a great effect on the surge, heave, and pitch motions of the platform. The trend of change is consistent with that of the motor displacement. When the orifice area increases to a certain level, the change in the orifice area has negligible effect on the surge, heave, and pitch motions of the platform. When the orifice area is small, increasing the orifice area gradually decreases the pressure difference between the two sides of the flow control valve. Increasing the orifice area will reduce the pressure at point b in the hydraulic PTO system, thereby decreasing the PTO reaction force on the platform. As the orifice area increases continuously, the pressure difference between the two sides of the flow control valve tends to zero. Continuing to increase the orifice area has negligible effect on the pressure at point b in the hydraulic PTO system.

In Fig. 9(e), (f), the surge motion of the platform remains essentially the same with increasing initial volume and pre-charge pressure, and is hardly affected by changes in these parameters. In Fig. 10(e), (f) and Fig. 11(e), (f), the heave and pitch motion of the platform gradually increases with the increase of initial volume and pre-charge pressure, and the increase is more greatly with a larger period.

In Fig. 9, when $T = 5$ s, the amplitude of surge motion response of the platform varies greatly with the change of piston area, equivalent damping, motor displacement, and orifice area. The maximum increase reaches 56.4 %. In Fig. 10, when $T = 9$ s, the amplitude of heave motion response of the platform varies greatly with the change of piston area, equivalent damping, motor displacement, and orifice area. The maximum increase reaches 168 %. In Fig. 11, when $T = 6$ s, the amplitude of pitch motion response of the platform varies greatly with the change of piston area, equivalent damping, motor displacement, and orifice area. The maximum increase reaches 127.3 %. Since the platform is subjected to the hydraulic PTO system reaction force and wave force with a close phase and size, it greatly affects the surge, heave, and pitch motion of the platform as the PTO reaction force varies. During these periods, changes in the hydraulic parameters of the PTO system cause drastic changes in the surge, heave, and pitch motions of the platform, which may affect the operational status and safety of the hybrid system.

In Figs. 9, 10, and 11, the hydraulic parameters have different effects on the variation trends of the surge, heave, and pitch motion responses of the platform at different periods. This is mainly due to the fact that the surge, heave, and pitch motion response depend on the phase and amplitude of the total PTO reaction force and the wave excitation force. The buoys in the WECs micro array are evenly distributed around the hybrid system platform. The phase and amplitude of the reaction force of the PTO system at asymmetric positions in the micro array are

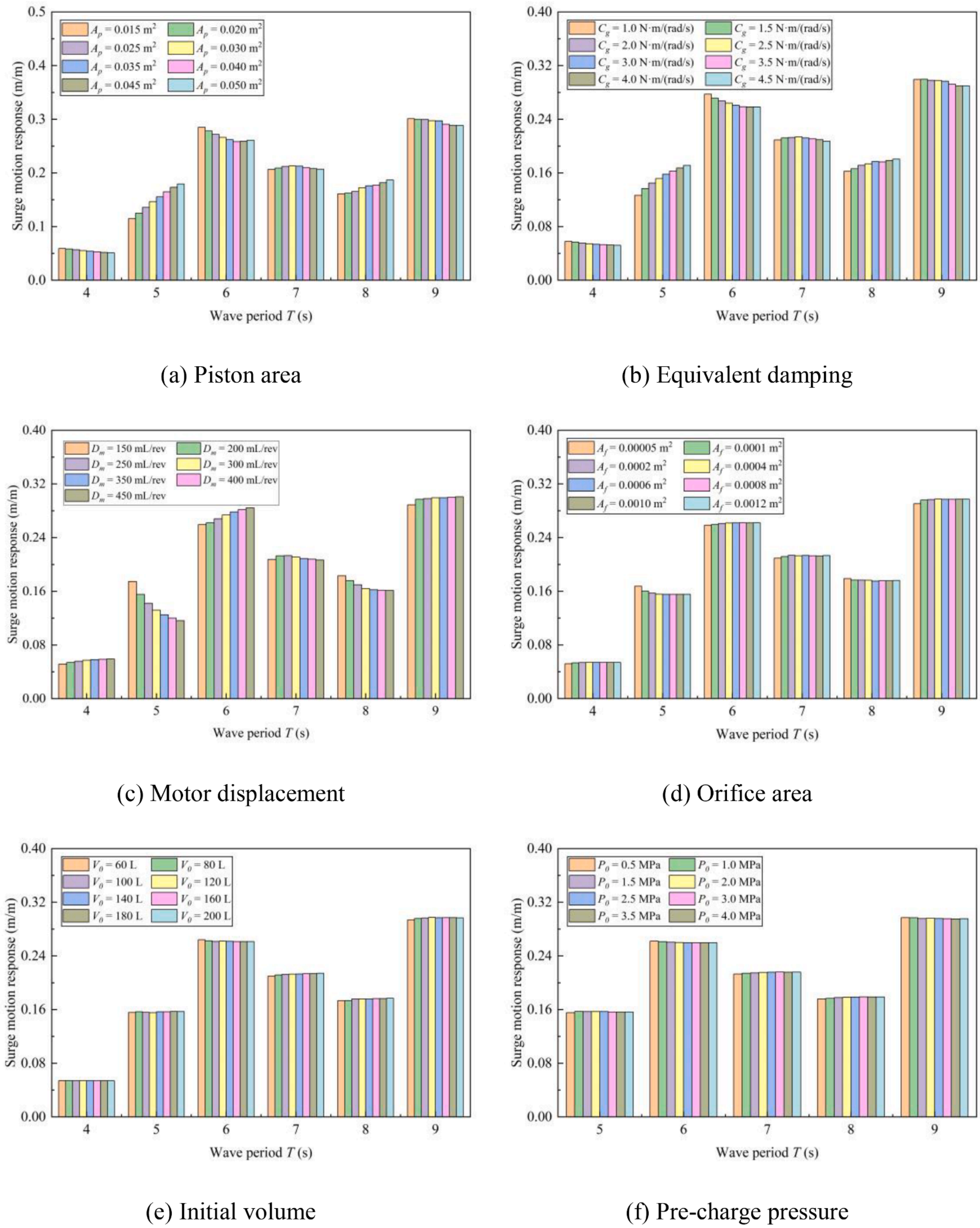

Fig. 9. The influence of hydraulic parameters on the surge motion.

different at different periods. One of the main goals of the proposed wind-wave hybrid system concept is to enhance platform stability through the WECs micro array. Therefore, the effects of the phase and amplitude of the hydraulic PTO reaction force on the platform motion are analyzed to provide a reference for the sway reduction control strategy of the wind-wave hybrid system.

Fig. 12 shows the PTO reaction moments and wave excitation moments on the platform when the hydraulic PTO system is at default parameters. In the figure, the platform is subjected to hydraulic PTO reaction moments and wave excitation moments that are cross-phase and of similar magnitude. In Fig. 12(a), (e), and (f), some of the hydraulic PTO reaction moments in the WECs micro array are of opposite phases but have similar amplitudes. The WECs micro array partially hydraulic PTO reaction moments and wave excitation moments in opposite phases. For example, in Fig. 12(a), the reaction moments of PTO1 and PTO3, as well as PTO4 (PTO7) and PTO5 (PTO6), are opposite in phase and close in amplitude. The wave excitation moments and the reaction moments of PTO8 are opposite in phase and close in amplitude. As the hydraulic parameters change, the PTO reaction moment and wave excitation moment cancel each other out, resulting in a relatively small change in the amplitude of the platform's pitch motion. In Fig. 12 (b), (c), and (d), the phases of the reaction moments are similar for most locations of the WECs micro array. Although some of the PTO reaction moments and wave excitation moments have opposite phases in some periods, other PTO reaction moments are close in phase. For example, in Fig. 12(c), PTO1, PTO2 (PTO2), PTO3 (PTO8), and PTO5 (PTO6)

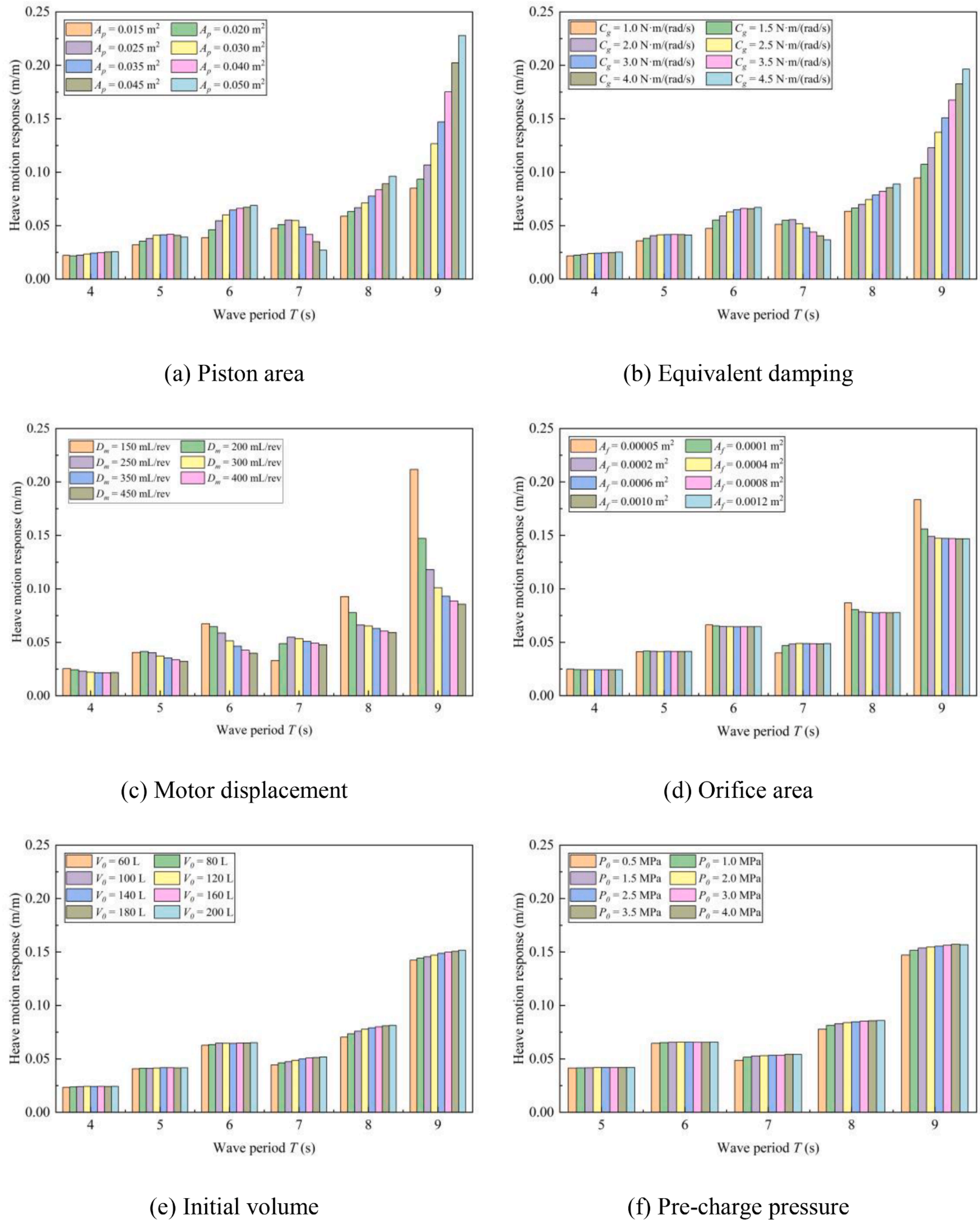

Fig. 10. The influence of hydraulic parameters on the heave motion.

reaction moments are close to each other in phase. The change of PTO reaction moments has a large influence on the pitch motion response, and the amplitude of the change of the pitch motion response is relatively large.

The piston area and equivalent damping in the hydraulic PTO system have similar effects on the surge, heave, and pitch motion responses, while the motor displacement and orifice area have opposite effects. They both change the PTO forces acting on the buoy and platform by changing the hydraulic PTO system pressure. Although piston area, equivalent damping, motor displacement, and orifice area can all affect the surge, heave, and pitch motions responses, the effects on the platform motion responses have different characteristics. The piston area of the hydraulic cylinder is not easily adjustable during the operation of the wind-wave hybrid system, which makes it challenging to reduce the pitch motion response by controlling the piston area. Since there is a lower limit to regulating the PTO system pressure by orifice area, there is also an upper limit to reducing the pitch motion response of the platform solely by controlling the orifice area. The motor displacement and equivalent damping can be adjusted to control the PTO system pressure over a wide range. By controlling the motor displacement and equivalent damping, the motion response of the platform can be reduced.

4.2. Effect on the WECs micro array power generation

The flow and pressure of hydraulic PTO system are influenced by hydraulic parameters that are associated with the power generation of

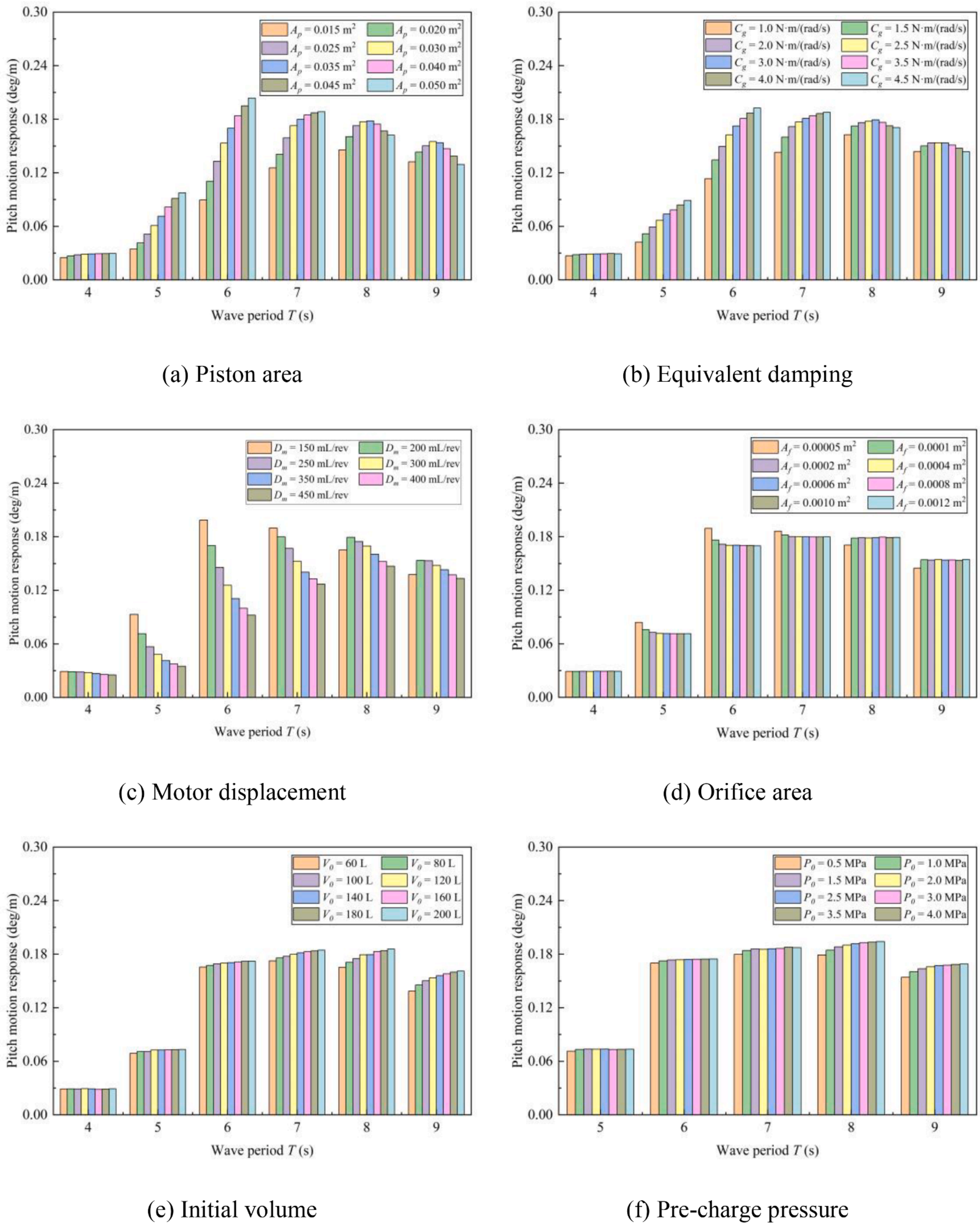

(a) Piston area (b) Equivalent damping

(c) Motor displacement (d) Orifice area

(e) Initial volume (f) Pre-charge pressure

Fig. 11. The influence of hydraulic parameters on the pitch motion.

WECs micro array. The effects of piston area, motor displacement, orifice area, equivalent damping, initial volume, and pre-charge pressure of the PTO system on the power generated by the WECs micro array are analyzed when the hydraulic parameters vary.

Fig. 13 shows the effect of hydraulic parameters on the power generation of WECs micro array. In Fig. 13(a) – (d), the piston area, equivalent damping, motor displacement, and orifice area have great effects on the power generation of WECs micro array. In Fig. 13(e) and (f), the initial volume and pre-charge pressure of the accumulator have a limited effect on the power generation of the WECs micro array.

In Fig. 13(a)-(c), when the wave period increases from 4 to 9 s, the output power of the WECs array is increasingly affected by variations in piston area, equivalent damping, and motor displacement parameters. When $T = 9$ s, the maximum variation amplitudes of the power generation of WECs micro array reach 450 %, 193.6 %, and −80.3 %, respectively. There is an optimal piston area, equivalent damping, and motor displacement to maximize the power generation of the WECs micro array. Although the power generation of the WECs micro array varies monotonously in some periods, this variation may be attributed to the limitation of the range of parameter values. In Fig. 13(d), the power generation of WECs micro array increases gradually with the increase of orifice area and finally stabilizes. When $T = 5$ s, the maximum increase in the power generation of WECs micro array reaches 43.9 %. During the process of increasing the orifice area, the pressure difference between points b and d in the PTO system gradually decreases. The energy loss generated at the valve opening gradually decreases, and the power

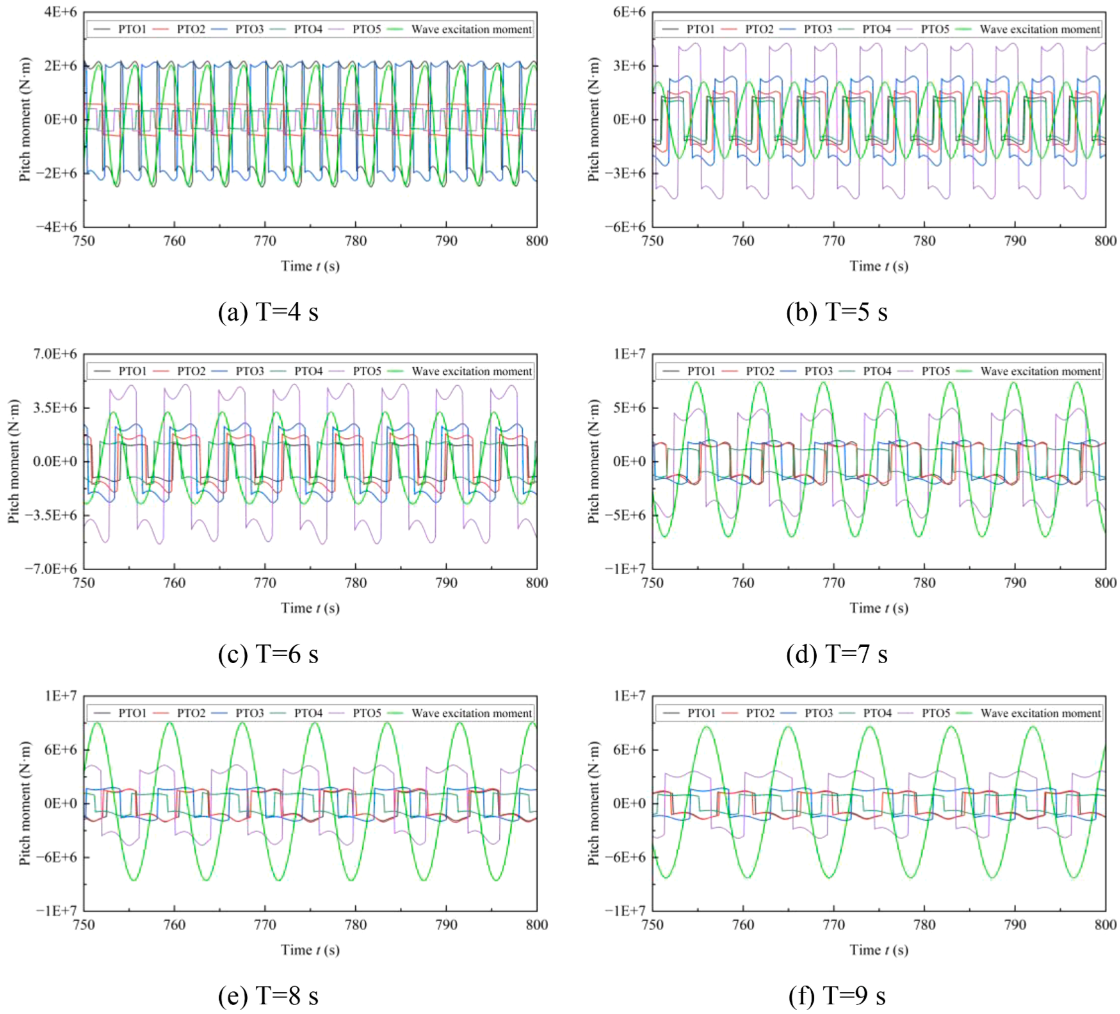

Fig. 12. Wave excitation moment and PTO reaction moments on platform with different periods.

generation of the WECs micro array gradually increases until it stabilizes.

In Fig. 13(e) and (f), the power generation of WECs micro array gradually increases with the initial volume and pre-charge pressure of the accumulator, and eventually stabilizes. When $T = 8$ s, the power generation of WECs micro arrays increases by 8.9 % and 5.1 %, respectively. When the initial volume or pre-charge pressure is small, the accumulator may not be able to completely absorb the flow and pressure pulsations within the PTO system. As the initial volume or pre-charge pressure of the accumulator increases, the flow and pressure within the PTO system tend to stabilize, and the power generation of WECs micro array tends to stabilize.

The piston area, equivalent damping, and motor displacement in hydraulic PTO system can all affect the power generated by WECs micro array over a wide range. The piston area is difficult to change during the actual operation of the wind-wave hybrid system. The power generation of the WECs micro array can be maximized by controlling the equivalent damping and motor displacement. The orifice area can also affect power generation of the WECs micro array over a wide range. However, it regulates the flow rate into the hydraulic motor through the pressure loss at both ends of the control valve, which does not apply to the maximum power generation control of WECs micro array. The accumulator acts as a pressure-stabilizing unit, and its initial volume and pre-charge pressure have a limited effect on the energy conversion of the PTO system.

Comparing the simulation results in Figs. 11 and 13, the pitch motion response of the platform is not at its minimum when the WECs micro array generates the maximum power at different periods. As the piston area, equivalent damping, motor displacement, and orifice area increase, it becomes nearly impossible to achieve both maximum power generation of the WECs micro array and minimize the pitch motion response of the platform in the wind-wave hybrid system simultaneously. Therefore, during the operation of the hybrid system, the appropriate motor displacement or equivalent damping is selected based on the actual requirements to meet the needs of the hybrid system for pitch motion response and WECs micro array power generation.

4.3. Effect on the wind turbine power generation and rotor torque

Hydraulic parameters influence the motion of the hybrid system platform, subsequently affecting the power generation and rotor torque of the wind turbine. The effects of piston area, motor displacement, orifice area, equivalent damping, initial volume, and pre-charge pressure on the power generation of WECs micro array in PTO systems are analyzed when the hydraulic parameters vary.

During the operation of the hybrid system, the surge and heave motions of the platform have less effect on the wind turbine, while the pitch motion greatly affects power generation and safety. In Fig. 11, the hydraulic parameters, such as piston area, equivalent damping, motor displacement, and orifice area, have the great effect on the pitch motion of the platform when the period $T = 5$, 6, 7 s, and 8 s. Therefore, the effect of hydraulic parameters on the power generation of the wind

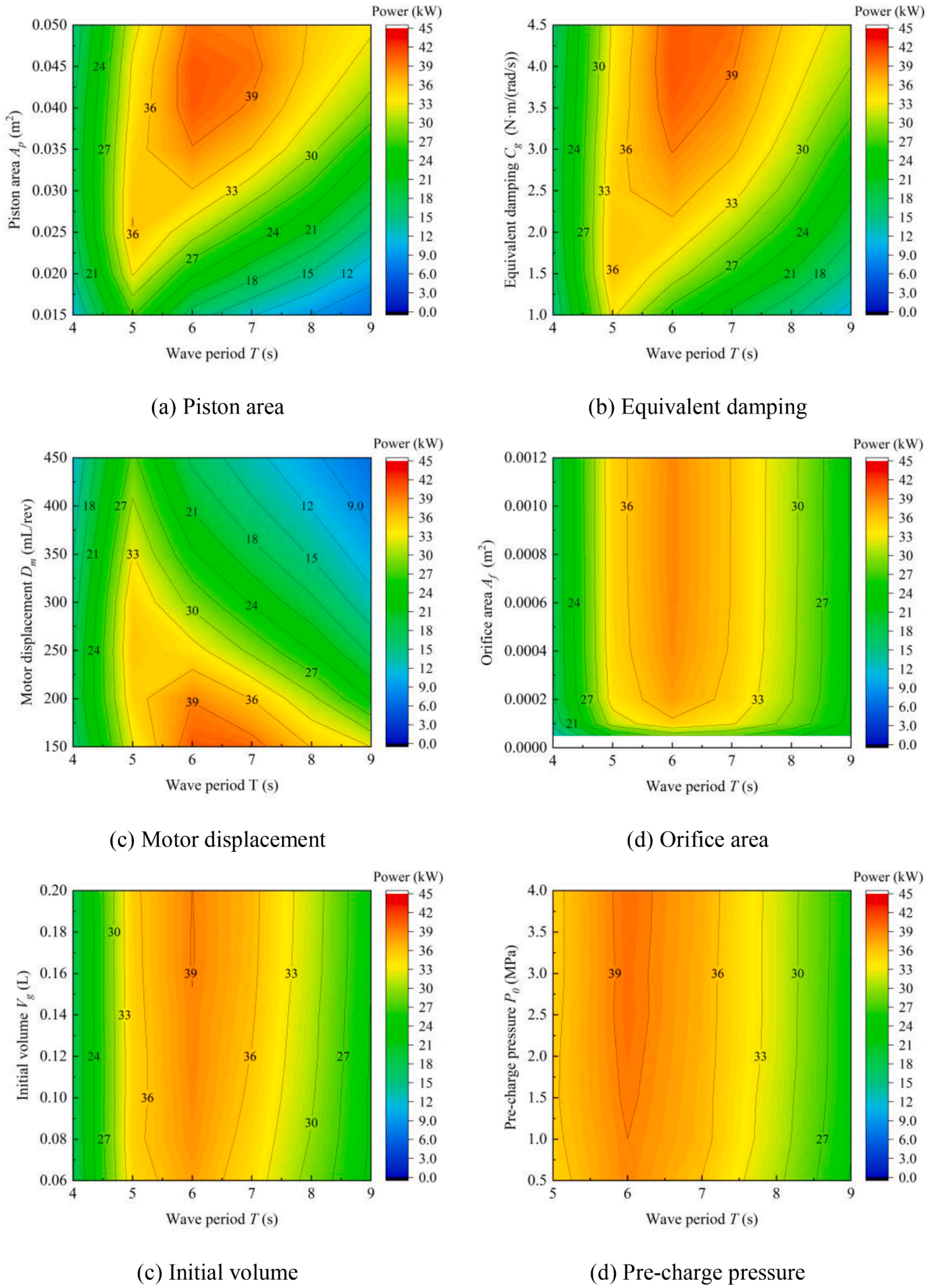

(a) Piston area (b) Equivalent damping

(c) Motor displacement (d) Orifice area

(c) Initial volume (d) Pre-charge pressure

Fig. 13. The influence of hydraulic parameters on the power generation of WECs micro array.

turbine is analyzed. In Fig. 14, the piston area, equivalent damping, motor displacement, and orifice area affect the amplitude of power generation ((max-min)/2) of the wind turbine, while the initial volume and pre-charge pressure have a negligible effect on the power generation amplitude of the wind turbine, which can be disregarded. The piston area, equivalent damping, motor displacement, orifice area, initial volume, and pre-charge pressure have a negligible effect on the average power generation of the wind turbine.

In Fig. 14(a) (b), the amplitude of power generation gradually increases as the piston area and equivalent damping increase. When $T = 5$ s, the amplitude of power generation increases by 82.9 % and 137.7 %, respectively. In Fig. 14(c) (d), the amplitude of the power generated gradually decreases as the motor displacement and orifice area increase. When $T = 5$ s, the amplitude of power generation decreases to 60.6 % and 10.4 %, respectively. This is mainly due to the changes in hydraulic parameters such as piston area, equivalent damping, motor

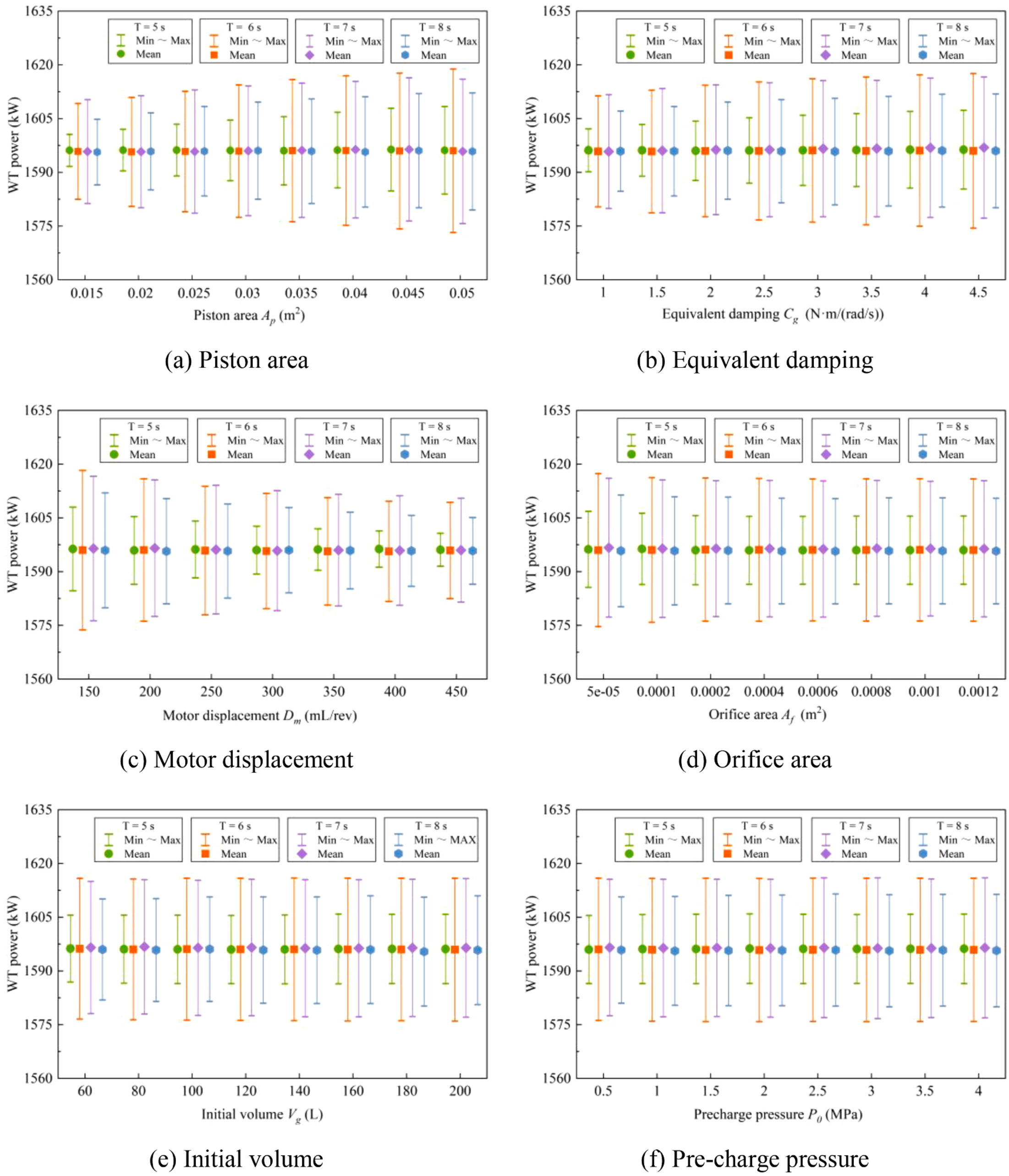

Fig. 14. The influence of hydraulic parameters on the power generation of wind turbine.

displacement, and orifice area, which affect the motion response of the platform. In Fig. 14(e) (f), the initial volume and pre-charge pressure of the accumulator have negligible effect on the amplitude of the power generation. When $T = 5$ s, the amplitude of power generation increased by 3.4 % and 2.1 %, respectively. The initial volume and pre-charge pressure of the accumulator have less effect on the platform motion, and the instantaneous maximum and minimum power of the wind turbine remain almost unchanged.

Fig. 15 shows the effect of hydraulic parameters on the rotor torque of the wind turbine. In Fig. 15, the piston area, equivalent damping, motor displacement, and orifice area influence the amplitude of rotor torque, while the initial volume and pre-charge pressure have negligible effect on the amplitude of rotor torque. In Fig. 15, the piston area, equivalent damping, motor displacement, orifice area, initial volume, and pre-charge pressure have negligible effect on the average rotor torque.

In Fig. 15(a), (b), the amplitude of rotor torque gradually increases with the increasing piston area and equivalent damping. When $T = 5$ s, the amplitude of rotor torque increases by 85.7 % and 183.3 %, respectively. In Fig. 15(c), (d), the amplitude of rotor torque gradually decreases with the increasing the motor displacement and orifice area. When $T = 5$ s, the amplitude of the rotor torque decreases by 66.1 % and 14.6 %, respectively. In Fig. 15(e) (f), the initial volume and pre-charge pressure of the accumulator have negligible effect on the amplitude of the rotor torque. When $T = 5$s, the amplitude of rotor torque increases by 4 % and 1.9 %. The wind speed of 7.63 m/s is lower than the rated wind speed. The wind turbine adopts a fixed-speed control strategy, and the instantaneous power of the wind turbine follows the same trend as the rotor torque.

As the piston area and equivalent damping increase, or the motor displacement and orifice area decrease, the pitch motion of the platform intensifies, expanding the amplitude of the wind turbine's generated power and rotor torque. Although the average power generation of the wind turbine has negligible effect, the amplitude of the power

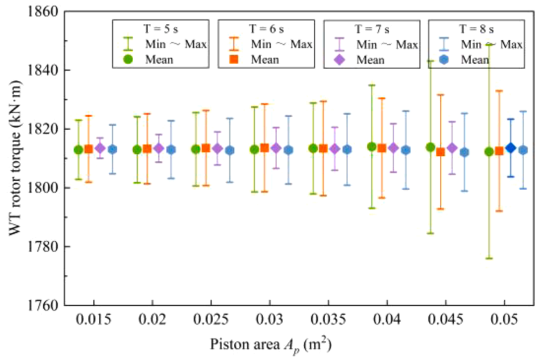

(a) Piston area

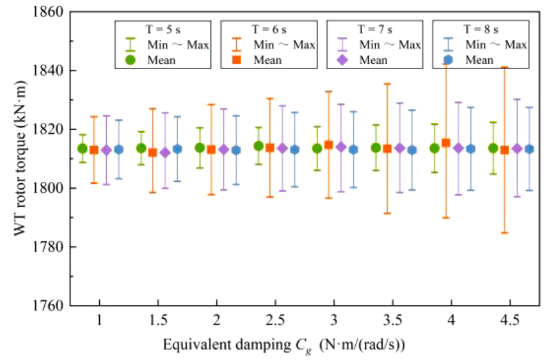

(b) Equivalent damping

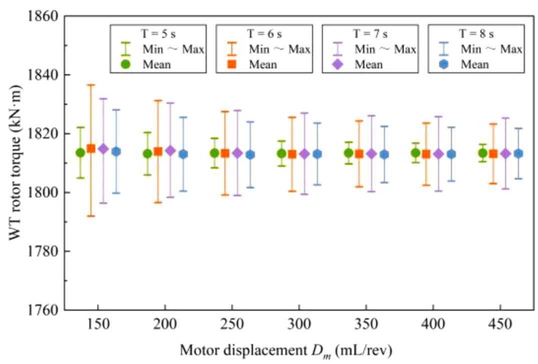

(c) Motor displacement

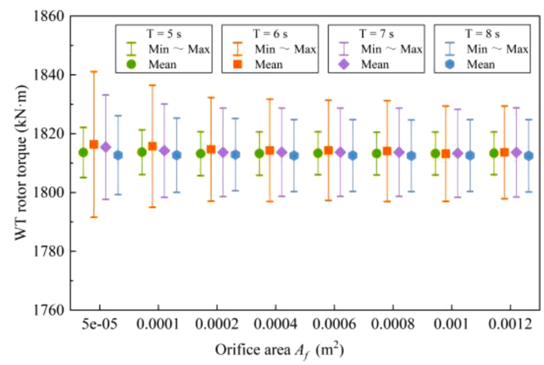

(d) Orifice area

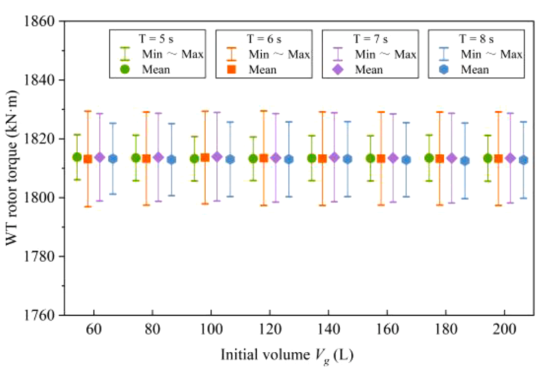

(e) Initial volume

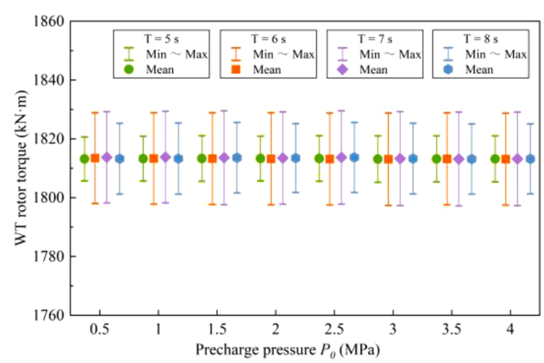

(f) Pre-charge pressure

Fig. 15. The influence of hydraulic parameters on rotor torque of wind turbine.

generation increases, which affects the quality of grid-connected power. The increased amplitude of rotor torque may lead to problems such as structural vibration and gear fatigue, ultimately resulting in irreversible losses.

5. Conclusions

This paper focuses on the wind-wave hybrid system and establishes an aero-hydro-servo-hydraulic-mooring full coupling simulation method. The study investigates the effects of parameter variations of typical components such as hydraulic cylinders, hydraulic motors, flow control valves, generators, and accumulators in the hydraulic PTO system on the platform motion response, natural period, power generation, and rotor torque of the hybrid system. The main results of the study are as follows:

1. The piston area, motor displacement, orifice area, and equivalent damping in the hydraulic PTO system have negligible effect on the platform surge natural period. However, they greatly affect the heave and pitch natural periods, and the maximum variation ranges are 14.2 % and 12.7 %. As the piston area and equivalent damping increase, the heave and pitch natural periods gradually decrease. The motor displacement and orifice area have opposite effects on the heave and pitch natural periods.

2. The piston area, motor displacement, orifice area, and equivalent damping in the hydraulic PTO system have great effects on the surge, heave, and pitch motion response of the platform. With changes in hydraulic parameters, the maximum increases in surge, heave, and pitch of the platform reached 56.4 %, 168 %, and 127.3 %, respectively. The effectiveness of WECs micro arrays in reducing the motion response of the platform depends on the phase and amplitude of the reaction and wave excitation forces of the hydraulic PTO system. In the same period, the piston area and equivalent damping have a similar effect on the surge, heave, and pitch motion response of the platform, while the motor displacement and orifice area have the opposite effect. The initial

volume and pre-charge pressure have negligible effect the surge motion response and non-negligible effect on the heave and pitch motion response of the platform, especially in the long period waves.

3. Variations in the parameters of the components of the PTO system, including the hydraulic cylinder, hydraulic motor, flow control valve, and generator, significantly affect the power generation of WECs micro array. For a determining sea state, there are optimal hydraulic parameters that maximize the power generation of the WECs micro arrays. The parameters of the accumulator, such as the initial volume and pre-charge pressure, have a little effect on the power generation of WECs micro array, especially when they are set at high values.

4. The wind-wave hybrid system is hard to reduce the pitch motion response of the platform and maximize the power generation of the WECs micro array simultaneously. By analyzing the influence of hydraulic parameters on the wind-wave hybrid system, the motor displacement and equivalent damping are suitable as control variables of the PTO system. During the operation of the wind-wave hybrid system, the hydraulic motor displacement or generator equivalent damping in the WECs micro array PTO system can be controlled according to the actual requirements to achieve either maximum power tracking control of the WECs micro array or reduced pitch motion response control of the platform.

5. Variations in the parameters of the components of the PTO system, including the hydraulic cylinder, hydraulic motor, flow control valve, and generator greatly affect the amplitudes of wind turbine power generation and rotor torque. In contrast, the parameters of the accumulator, such as the initial volume and pre-charge pressure, have negligible effect on the amplitudes of wind turbine power generation and rotor torque. All six hydraulic parameters have negligible effect on the average of power generation and rotor torque.

In this study, we develop an aero-hydro-servo-hydraulic-mooring fully coupled simulation method to facilitate the integrated development of offshore wind and wave energy. The effects of hydraulic parameters (i.e., the piston area, motor displacement, orifice area, equivalent damping, initial volume, and pre-charge pressure) on the output power and motion response of the hybrid system are analyzed by this method. The results show that the piston area, motor displacement, throttle orifice area, and equivalent damping significantly affect the power output and motion response of the hybrid system. In contrast, the initial volume and pre-charge pressure have a negligible influence. Because the hydrodynamic calculations of the hybrid system are based on potential flow theory, the effects of fluid viscosity are not considered. In future studies, we will incorporate viscosity corrections to further improve the model and further investigate control methods for maximizing power tracking of the WEC microarray, as well as reducing the pitch motion response of the platform.

CRediT authorship contribution statement

Tiesheng Liu: Writing – original draft, Validation, Software, Methodology, Formal analysis. **Yanjun Liu:** Resources, Investigation, Funding acquisition. **Shuting Huang:** Writing – review & editing, Funding acquisition. **Gang Xue:** Writing – review & editing, Resources, Funding acquisition.

Declaration of competing interest

The authors declare that they have no known competing financial interests or personal relationships that could have appeared to influence the work reported in this paper.

Funding

The research was supported by National Key R&D Program of China (2023YFB4204103), Natural Science Foundation of Shandong Province (ZR2021ZD23), National Natural Science Foundation of China (52201328), National Natural Science Foundation of China (52171265), Guangdong Basic and Applied Basic Research Foundation (2021A1515110687), National Key R&D Program of China (2023YFC2810100).

References

Ansys, A., 2021. AQWA Theory Manual [J]. AQWA, Canonsburg, PA, USA.
Astariz, S., Iglesias, G., 2015. The economics of wave energy: a review[J]. Renew. Sustain. Energy Rev. 45, 397–408.
Bevilacqua G., Zanuttigh B. Overtopping Wave Energy Converters: general aspects and stage of development[J]. 2011.
Blanco, M.I, 2009. The economics of wind energy[J]. Renew. Sustain. Energy Rev. 13 (6–7), 1372–1382.
Borg, M., Collu, M., Brennan, F.P., et al., 2013. Use of a wave energy converter as a motion suppression device for floating WTs. Energy Procedia 223–233.
Chen, M., Xiao, P., Zhou, H., et al., 2022. Fully coupled analysis of an integrated floating wind-wave power generation platform in operational sea-states [J]. Front. Energy Res. 10, 931057.
Chen, Z., Sun, J., Yang, J., et al., 2024. Experimental and numerical analysis of power take-off control effects on the dynamic performance of a floating wind-wave combined system[J]. Renew. Energy 226, 120353.
Cruz, J., 2007. Ocean Wave energy: Current Status and Future prespectives[M]. Springer Science & Business Media.
Cummins W.E. The impulse response function and ship motions [J]. 1962.
Falcão, AFO., 2007. Modelling and control of oscillating-body wave energy converters with hydraulic power take-off and gas accumulator[J]. Ocean Eng. 34 (14–15), 2021–2032.
Gao, Z., Moan, T., Wan, L., et al., 2016. Comparative numerical and experimental study of two combined wind and wave energy concepts [J]. J. Ocean Eng. Sci. 1 (1), 36–51.
Ghafari, H.R., Ghassemi, H., He, G., 2021b. Numerical study of the Wavestar wave energy converter with multi-point-absorber around DeepCwind semisubmersible floating platform [J]. Ocean Eng. 232, 109177.
Ghafari, H.R., Ghassemi, H., Neisi, A., 2022. Power matrix and dynamic response of the hybrid WavestarDeepCwind platform under different diameters and regular wave conditions [J]. Ocean Eng. 247, 110734.
Ghafari, H.R., Neisi, A., Ghassemi, H., et al., 2021a. Power production of the hybrid Wavestar point absorber mounted around the Hywind spar platform and its dynamic response[J]. J. Renew. Sustain. Energy 13 (3).
Han, M., Shi, H., Cao, F., et al., 2024. Dynamic characteristics and parameter analysis of a floating hybrid wind-wave energy system based on a novel coupled numerical framework[J]. Energy Convers. Manage 312, 118558.
Hess, J.L., Smith, AMO., 1967. Calculation of potential flow about arbitrary bodies[J]. Progr. Aerosp. Sci. 8, 1–138.
Huang, S., Wang, J., Yang, M., et al., 2024. Parameter analysis and dual-objective optimization of the hydraulic power take-off system of a floating wind-wave hybrid system[J]. Ocean Engineering 307, 118058.
Inoue, M., Kaneko, K., Setoguchi, T., et al., 1987. Hysteretic characteristics of Wells turbine in reciprocating flow[J]. Nippon Kikai Gakkai Ronbunshu, B Hen;(Japan) 496.
Jin, P., Zheng, Z., Zhou, Z., et al., 2023. Optimization and evaluation of a semi-submersible wind turbine and oscillating body wave energy converters hybrid system [J]. Energy 282, 128889.
Jonkman, J.M., Hayman, G.J., Jonkman, B.J., et al., 2015. AeroDyn v15 user's guide and theory manual[J]. NREL Draft Rep. 46.
Kamarlouei, M., Gaspar, J.F., Calvario, M., Hallak, T.S., Soares, C.G., 2020. Experimental analysis of wave energy converters concentrically attached on a floating offshore platform. Renew.Energy 152, 1171–1185.
Khurshid, H., Mohammed, B.S., Al-Yacoubya, A.M., et al., 2024. Analysis of hybrid offshore renewable energy sources for power generation: a literature review of hybrid solar, wind, and waves energy systems[J]. Dev. Built Environ., 100497
Kim, S.J., Koo, W., Shin, M.J, 2019. Numerical and experimental study on a hemispheric point-absorbertype wave energy converter with a hydraulic power take-off system [J]. Renew. Energy 135, 1260–1269.
Konispoliatis, D.N., Katsaounis, G.M., Manolas, D.I., et al., 2021. REFOS: a renewable energy multi-purpose floating offshore system[J]. Energies. (Basel) 14 (11), 3126.
Legaz, M.J., Coronil, D., Mayorga, P., et al., 2018. Study of a hybrid renewable energy platform: w2Power[C]. In: //International Conference on Offshore Mechanics and Arctic Engineering. American Society of Mechanical Engineers, p. 51326. V11AT12A040.
Leijon, M., Danielsson, O., Eriksson, M., et al., 2006. An electrical approach to wave energy conversion[J]. Renew. Energy 31 (9), 1309–1319.
Liu, C., Yang, Q., Bao, G, 2018. Influence of hydraulic power take-off unit parameters on power capture ability of a two-raft-type wave energy converter [J]. Ocean Eng. 150, 69–80.
Liu, T., Liu, Y., Huang, S., et al., 2024. Optimization of wind-wave hybrid system based on wind-wave coupling model [J]. IET Renew. Pow. Gener.
Michailides, C., Gao, Z., Moan, T., 2016. Experimental study of the functionality of a semisubmersible wind turbine combined with flap-type Wave Energy Converters[J]. Renew. Energy 93, 675–690.
Moriarty P.J. AeroDyn Theory Manual[R]. Technical Report, NREL/TP-500-36881, 2005.

Muliawan, M.J., Karimirad, M., Gao, Z., et al., 2013. Extreme responses of a combined spar-type floating wind turbine and floating wave energy converter (STC) system with survival modes[J]. Ocean Eng. 65, 71–82.
Newman, J.N, 2018. Marine hydrodynamics[M]. The MIT press.
Perez-Collazo, C., Pemberton, R., Greaves, D., et al., 2019. Monopile-mounted wave energy converter for a hybrid wind-wave system[J]. Energy Convers. Manage 199, 111971.
Roddier, D., 2011. A generic 5 MW WindFloat for numerical tool validation & comparison against a generic spar[J]. OMAE2011-50278.
Roddier, D., Banister, K., 2012. WindWaveFloat (WWF): Final Scientific Report[R]. Principle Power Inc., Seattle, WA United States.
Roddier, D., Cermelli, C., Aubault, A., et al., 2010. WindFloat: a floating foundation for offshore wind turbines[J]. J. Renew. Sustain. Energy 2 (3).
Rony, J.S., Karmakar, D., 2023. Performance of a hybrid TLP floating wind turbine combined with arrays of heaving point absorbers[J]. Ocean Eng. 282, 114939.
Rony, J.S., Karmakar, D., 2024. Hydrodynamic response analysis of a hybrid TLP and heaving-buoy wave energy converter with PTO damping[J]. Renew. Energy 226, 120380.
Rusu, E., Onea, F., 2018. A review of the technologies for wave energy extraction[J]. Clean Energy 2 (1), 10–19.
Si, Y., Chen, Z., Zeng, W., et al., 2021. The influence of power-take-off control on the dynamic response and power output of combined semi-submersible floating wind turbine and point-absorber wave energy converters[J]. Ocean Eng. 227, 108835.
So, R., Simmons, A., Brekken, T., et al., 2015. Development of pto-sim: a power performance module for the open-source wave energy converter code wec-sim[C]//. International Conference on Offshore Mechanics and Arctic Engineering. American Society of Mechanical Engineers 56574. V009T09A032.
Sricharan, V.V.S., Chandrasekaran, S, 2021. Time-domain analysis of a bean-shaped multi-body floating wave energy converter with a hydraulic power take-off using WEC-Sim [J]. Energy 223, 119985.
Stock, A., 2024. Accounting for power take-off efficiency in optimal velocity tracking control of wave energy converters[J]. Ocean Eng. 312, 119191.
Taveira-Pinto, F., Rosa-Santos, P., Fazeres-Ferradosa, T., 2020. Marine renewable energy [J]. Renew. Energy 150, 1160–1164.
Turkenburg, W., Arent, D.J., Bertani, R., et al., 2012. Renewable Energy. Global Energy Assessment: Toward a Sustainable Future. Cambridge University Press, pp. 761–900.
Wan, L., Moan, T., Gao, Z., et al., 2024. A review on the technical development of combined wind and wave energy conversion systems[J]. Energy, 130885.
Yang, Y., Bashir, M., Michailides, C., et al., 2020. Development and application of an aero-hydro-servo-elastic coupling framework for analysis of floating offshore wind turbines[J]. Renew. Energy 161, 606–625.
Yao, G., Luo, Z., Lu, Z., et al., 2023. Unlocking the potential of wave energy conversion: a comprehensive evaluation of advanced maximum power point tracking techniques and hybrid strategies for sustainable energy harvesting[J]. Renew. Sustain. Energy Rev. 185, 113599.
Zhang, D., Chen, Z., Liu, X., et al., 2022. A coupled numerical framework for hybrid floating offshore wind turbine and oscillating water column wave energy converters [J]. Energy Convers. Manage 267, 115933.
Zhu, H., Hu, C., Sueyoshi, M., et al., 2020. Integration of a semisubmersible floating wind turbine and wave energy converters: an experimental study on motion reduction[J]. J. Mar. Sci. Technol. 25, 667–674.
Zhu, K., Cao, F., Wang, T., et al., 2024. A comparative investigation into the dynamic performance of multiple wind-wave hybrid systems utilizing a full-process analytical model[J]. Appl. Energy 360, 122761.